

Published in final edited form as:

Nat Med. 2016 December ; 22(12): 1428–1438. doi:10.1038/nm.4222.

Cardioprotection and lifespan extension by the natural polyamine spermidine

A full list of authors and affiliations appears at the end of the article.

Abstract

Aging is associated with an increased risk of cardiovascular disease and death. Here we show that oral supplementation of the natural polyamine spermidine extends the lifespan of mice and exerts cardioprotective effects, reducing cardiac hypertrophy and preserving diastolic function in old mice. Spermidine feeding enhanced cardiac autophagy, mitophagy and mitochondrial respiration, and it also improved the mechano-elastic properties of cardiomyocytes in vivo, coinciding with increased titin phosphorylation and suppressed subclinical inflammation. Spermidine feeding failed to provide cardioprotection in mice that lack the autophagy-related protein Atg5 in cardiomyocytes. In *Dahl* salt-sensitive rats that were fed a high-salt diet, a model for hypertension-induced congestive heart failure, spermidine feeding reduced systemic blood pressure, increased titin phosphorylation and prevented cardiac hypertrophy and a decline in diastolic function, thus delaying the progression to heart failure. In humans, high levels of dietary spermidine, as assessed from food questionnaires, correlated with reduced blood pressure and a lower incidence of cardiovascular disease. Our results suggest a new and feasible strategy for the protection from cardiovascular disease.

Introduction

Cardiovascular disease has reached epidemic proportions in the elderly and remains the worldwide leading cause of death. Human aging is typically accompanied by cardiac hypertrophic remodeling and a progressive decline of left ventricular (LV) diastolic function^{1,2}. Abnormal diastolic function is present in >20% of the population >65 years of age³. Although less than half of all patients with diastolic dysfunction show clinical signs of

Correspondence should be addressed to: frank.madeo@uni-graz.at, simon.sedej@medunigraz.at, or kroemer@orange.fr.

*These authors contributed equally

#These authors jointly directed this work.

Author Contributions

T.E., S. Sedej, G.K. and F.M. designed and supervised the study; T.E., M.A., G.K., S. Sedej, and F.M. wrote the manuscript. T.E., M.A., S. Schroeder, U.P., S. Stekovic, T. Pendl, A.H., J. Schipke, A.Z., A.S., M.T., C.R., C.D., A.S.G., V.H., C.Ma., G.T., S.N., A.M., Z.H., A.K., D.C.-G., S.B., F.P., O.K., E.S., P.R., C.S., A.R., M.H., F.N., D.J., B.R., J.R., T.M., M.M., P.W., M.v.F.-S., R.P. and S.Sedej performed experiments, analyzed and discussed data. K.E., K.M., J.B., H.F., V.G.-D., M.H.d.A., G.H., B.P., L.S., T. Pieber, J.W., S.J.S., W.A.L., C. Mühlfeld, J. Sadoshima, J.D., and S.K. discussed & analyzed data and gave conceptual advice.

Competing Financial Interests

F.M., T.E., D.C.-G., S.J.S. and S. Stekovic. have equity interests in TLL, a company founded in 2016 that will develop natural food extracts.

Accession Codes

Array data are available via Gene Expression Omnibus (GEO) database with identifier GSE86882. Proteome data are available via ProteomeXchange with identifier PXD004916.

congestive heart failure, even patients not meeting the diagnostic criteria are at increased risk to develop heart failure⁴. No treatment has yet been shown to convincingly target and prevent age-associated diastolic dysfunction or heart failure, likely because our understanding of the fundamental mechanisms underlying progressive deteriorations in the (ultra-)structure and function of the aging heart is incomplete.

Recent studies have revealed that autophagy, a major cellular quality control mechanism, may be able to minimize the functional decline of aging cardiomyocytes by degrading and recycling long-lived proteins, which are potentially toxic if damaged, as well as cytoplasmic components and dysfunctional organelles (in particular, damaged mitochondria)^{5,6}. Clearance of dysfunctional mitochondria through a specific type of selective autophagy, termed mitophagy, may be beneficial for cardiac function, because mitochondria can overproduce reactive oxygen species if they are functionally impaired and ignite lethal signalling pathways if they are permeabilized. In view of the established longevity-extending effects of enhanced cytoprotective autophagy in model organisms, it seems plausible that autophagy might also be able to counteract cardiac aging⁷. We previously discovered that the natural polyamine spermidine, a dietary compound, extends lifespan and health span through induction of autophagy in yeast, flies and worms^{8,9}. Dietary supplementation of spermidine delayed age-associated memory impairment in flies¹⁰, prevented motor impairment in flies elicited by transgenic expression of human α -synuclein¹¹, and protected mice from TDP-43-associated proteinopathies¹², in line with a general neuroprotective action of this polyamine. In several model organisms, the lifespan extending and neuroprotective effects of spermidine were abolished upon inactivation of essential autophagy-related genes^{8,10}. Here, we explored the potential cardioprotective effects of spermidine in rodent models of physiological cardiac aging (mice) and high salt-induced congestive heart failure (rats). We also provide evidence that dietary spermidine intake in humans inversely correlates with cardiovascular disease.

Results

Spermidine extends the lifespan of wild-type C57BL/6 mice

In view of the life prolonging effects of spermidine in model organisms^{8,9}, we tested the long-term survival effects of specific polyamines in C57BL/6J wild-type female mice, which had a *life-long* (Fig. 1a) access to drinking water supplemented with distinct polyamines. Strikingly, spermidine- or spermine-supplemented mice had a significantly extended median lifespan as compared to control (receiving normal drinking water) or putrescine-supplemented mice (Fig. 1b, c and Supplementary Tables 1 and 2). To enhance the translational potential of these findings, we administered spermidine *late-in-life*, (a regimen more applicable to humans) to pre-aged male and female mice (Fig. 1a). Again, we found that spermidine feeding significantly prolonged median lifespan by ~10% (Fig. 1d and Supplementary Fig. 1). Spermidine-fed animals displayed increased circulating spermidine levels, confirming its systemic bioavailability (Fig. 1e). Food and water consumption, body weight and lean/fat mass composition were similar in spermidine-fed and control groups (Supplementary Fig. 2), excluding the possibility that polyamine supplementation extends lifespan by inducing a calorically-restricted state¹³.

Dietary spermidine delays cardiac aging by improving diastolic function

Tumor burden and cardiac aging are significant predictors of mortality in C57BL/6 mice and humans^{14,15}. Comprehensive pathological characterization of tissues collected from mice at an advanced age (28 months), as well as from old mice that became moribund and were sacrificed as “end-of-life” animals¹⁶, revealed similarly high tumor frequencies in spermidine-treated and control mice (Supplementary Fig. 3 and Supplementary Tables 3, 4). This finding suggests that the potential ability of spermidine to inhibit tumor formation, which has been observed after chemo-induction of tumors¹⁷, does not explain its life prolonging effects.

Since only minor histopathological abnormalities were observed in cardiac tissue obtained from 28-month-old or from “end-of-life” animals (Supplementary Tables 3, 4), we next subjected aged mice with *late-in-life* spermidine supplementation to structural and functional cardiac phenotyping. Spermidine reversed age-associated (23 months) echocardiography-detectable hypertrophy, as indicated by a reduction in tibia length-normalized left ventricular mass (LV mass/TL) and posterior wall thickness (PW/TL) to values below those observed in middle-aged (18 months) wild-type mice (Fig. 1f, Supplementary Table 5). Hypertrophic remodeling is the most common age-related myocardial abnormality that is associated with diastolic and/or systolic dysfunction, eventually leading to heart failure in humans¹⁸. Evaluation of cardiac function by invasive hemodynamic pressure-volume measurements revealed that compared with age-matched control mice, mice fed spermidine *late-in-life* had significantly enhanced diastolic properties, as reflected by a reduction of LV end-diastolic pressure (EDP; Fig. 1g, h) with a trend towards improved active relaxation (shortened time constant of LV pressure decay τ ; Supplementary Table 6), as well as significantly reduced LV passive stiffness, as reflected by decreased myocardial stiffness constant β (Fig. 1i), with a downward shift of the end-diastolic pressure-volume relationship [EDPVR] obtained by transient *vena cava* occlusion for load-independent cardiac function assessment (Supplementary Fig. 4). The systolic properties of aged hearts were less affected by spermidine. Load-dependent parameters, such as ejection fraction (EF) and dP/dt_{max} as indicators of LV contractility, were comparable in all tested groups (Fig. 1j, Supplementary Tables 5, 6). However, ventricular-vascular coupling (VVC), a parameter that describes the interaction of the LV with the arterial system, is positively correlated with cardiovascular performance and is associated with prognosis in heart failure patients¹⁹, was increased in mice fed spermidine *late-in-life* and was similar to the value observed in young mice (Fig. 1k). Notably, spermidine did not affect systemic systolic and diastolic blood pressure (Fig. 1l), indicating that reduced hypertrophic remodeling, improved VVC and enhanced cardiac function were independent of arterial afterload. Moreover, 24-month-old control mice displayed a moderate but significant increase in relative lung weight (LW/TL), a sign of pulmonary congestion that results from abnormal diastolic function, as compared to that in young animals (Supplementary Table 7). This age-dependent increase in relative lung weight was less pronounced and was non-significant in spermidine-treated animals (Supplementary Table 7). Despite the evidence for pulmonary congestion, a typical complication in heart failure, in physiologically aged C57BL/6 mice, these mice are not considered to represent an experimental model of heart failure²⁰. Old C57BL/6 mice exhibit diastolic dysfunction with an increased risk for the

development of heart failure, thus closely recapitulating human cardiac aging in the absence of hypertension and associated comorbidities²⁰.

Cardiomyocyte composition and function are improved by spermidine

In the elderly patient, cardiac hypertrophy is related to structural and functional remodeling that may involve (i) changes in the composition and structure of the extracellular matrix, mainly characterized by fibrotic (collagen-rich) tissue; (ii) altered coronary microvascular rarefaction; and/or (iii) effects on cardiomyocytes themselves²¹. To test if spermidine reverses age-induced cardiac fibrosis and decreased coronary microvascular density, we subjected the hearts of aged mice fed spermidine *late-in-life* to ultrastructural analysis by design-based stereology. Electron microscopy did not reveal changes in the volume fraction or absolute volume of collagen, interstitium, capillaries or cardiomyocytes in the LV (Supplementary Fig. 5a and Supplementary Table 8). However, age-related effects on subcellular cardiomyocyte composition were reversed by spermidine, as reflected by increased relative mitochondrial and myofibrillar volumes and a reduced (mitochondria- and myofibril-free) sarcoplasmic volume (Fig. 2a, b, Supplementary Fig. 5b and Supplementary Table 8). These results suggest that spermidine has cardiomyocyte-intrinsic effect. We hypothesized that the increased myocardial compliance (i.e. myocardial elasticity) induced by spermidine originates from improved contractile apparatus and cardiomyocyte function²². Consistent with this idea, both transcriptome and proteome analyses of cardiac tissue extracts (Supplementary Fig. 6 and Supplementary Tables 9, 10) revealed a rejuvenated molecular phenotype with respect to components of the cytoskeletal apparatus (i.e. myosin heavy chain proteins, ankyrins, integrins, dystonin), inflammatory processes and mitochondrial respiratory chain complex I proteins (i.e. members of the Nduf protein family), all of which are essential for cardiomyocyte mechano-elastic functionality²³ and healthy cardiac aging^{24,25}. Accordingly, the respiratory competence of cardiac mitochondria through respiratory chain complex I was increased in mice supplemented with spermidine as compared to control mice (Fig. 2c, Supplementary Fig. 7a, b); thus, spermidine reversed an age-induced decline in mitochondrial respiratory function²⁶. Furthermore, spermidine reversed the age-associated decline of the mitochondria-related metabolite levels, including that of NADPH and mevalonate (Supplementary Fig. 7c-e), of which the latter has been linked to mitochondrial surveillance²⁷ and cardiac health²⁸. Moreover, determination of the (chronic) low-grade inflammatory status of aged mice (*see Methods*) revealed that spermidine reduced the age-dependent rise in plasma levels of the pro-inflammatory cytokine tumor necrosis factor- α (TNF α) (Fig. 2d, Supplementary Fig. 8). The passive stiffness of cardiomyocytes is determined primarily by titin-related mechanisms²², which are negatively affected by inflammatory conditions, in part mediated by TNF α ²⁹. Cardiomyocytes co-express a larger (more compliant) and a smaller (stiffer) isoform of titin, termed N2BA and N2B, respectively. While the isoform composition of titin, as assessed by the N2BA/[N2B+N2BA] ratio, was unchanged (Fig. 2e, f), spermidine enhanced the levels of both total and serine 4080 phosphorylation of the N2B isoform (Fig. 2e, g, Supplementary Fig. 5c). Phosphorylation of N2B on serine 4080 is known to reduce cardiomyocyte stiffness via cGMP/PKG-dependent signalling²².

Spermidine enhances cardiomyocyte autophagic flux in both young and aged mice

We previously identified spermidine as a potent inducer of autophagy^{8,9}, a cellular process crucial for general proteostasis as well as mitochondrial and cardiomyocyte function⁵. Therefore, we next tested whether spermidine supplementation improves autophagic flux in aging cardiomyocytes. To assess basal autophagic flux, we treated *ad libitum*-fed 13-month-old C57BL/6J wild-type mice supplemented with spermidine for the final four weeks with the vacuolar protease inhibitor leupeptin, which blocks autophagosome turnover, and quantified levels of the autophagosomal marker LC3-II³⁰. Treatment with leupeptin induced a significant increase of LC3-II levels in hearts from spermidine-supplemented mice, whereas age-matched controls showed a reduced (and non-significant) elevation of this marker (Fig. 3a, Supplementary Fig. 9e), indicating that spermidine increases cardiac autophagic flux *in vivo*. Cellular spermidine content in cardiac tissue was significantly increased in spermidine-supplemented animals as compared to controls (Fig. 3b).

The capacity of orally supplemented spermidine to induce autophagic flux *in vivo* in cardiomyocytes was corroborated by using transgenic cardiomyocyte-specific tandem-fluorescent mRFP-GFP-LC3 mice³¹. These mice serve as an autophagy reporter strain, carrying labeled autophagosomes; both red (mRFP) and green (GFP) fluorescence, as well as labeled autolysosomes; red (mRFP) fluorescence only. In this experiment, chloroquine was used to block autophagosome turnover for assessment of autophagic flux. Spermidine substantially increased the number of autophagosomes and autolysosomes under both vehicle- and chloroquine-treated conditions (Fig. 3c, d). Moreover, spermidine stimulated mitophagy in cardiomyocytes of both young and aged mice, as assessed in mice expressing the mitochondrial-targeted form of the fluorescent biosensor Keima (Mito-Keima). Mito-Keima fluorescence shows pH-dependent excitation characteristics, shifting excitation maxima to a higher wavelength after mitochondria come into contact with the acidic milieu of lysosomes in the context of mitophagy³². Thus, the ratio of 561 nm to 457 nm excited Keima fluorescence (referred to as Mito-Keima positive area) increases with a drop in pH (Online Methods). Spermidine treatment clearly increased the Mito-Keima-positive area in cardiomyocytes—indicative of increased mitophagy (Fig. 3e and Supplementary Fig. 9a-d). Together, these results suggest that autophagy may contribute to the improved cardiomyocyte structure and function induced by spermidine.

Autophagy is required for spermidine-mediated cardioprotection

To determine whether the *in vivo* cardioprotective effects of spermidine depend on autophagy, we took advantage of mice that have a cardiomyocyte-specific autophagy defect, *Atg5^{fl/fl}-MLC2a-Cre⁺* mice (*Atg5^{-/-}*)^{5,6}. We first verified that cardiomyocytes in these mice lack LC3-II and show increased levels of p62/SQSTM1, a direct target/substrate and cargo-receptor of autophagy known to increase in autophagy-deficient cardiomyocytes (Supplementary Fig. 10a-c). As these mice develop severe systolic impairment and heart failure early in life and do not reach the same age as wild-type animals^{5,6}, we assessed cardiac function at 16 weeks of age, when *Atg5^{-/-}* animals showed no echocardiography-detectable cardiac abnormalities under control conditions (Fig. 3f, g and Supplementary Table 11) and had systolic and diastolic properties that were comparable to those of *Atg5^{fl/fl}-MLC2a-Cre⁻* control mice (*Atg5^{+/+}*), as evaluated by invasive hemodynamics (Fig. 3h-k;

Supplementary Fig. 10d, e and Supplementary Table 11-13). Strikingly, the spermidine-induced reduction of LV hypertrophy (i.e. reduction of LVmass/TL and PW/TL) observed in *Atg5^{+/+}* mice was not detected in *Atg5^{-/-}* mice, in which spermidine actually aggravated LV hypertrophy (Fig. 3f and Supplementary Table 11). This increased LV hypertrophy in spermidine-treated *Atg5*-deficient mice was associated with reduced diastolic function, as documented by a significantly elevated EDPVR β , indicative of increased LV passive stiffness (Fig. 3i; Supplementary Fig. 10d and Supplementary Table 12). Notably, significant increases in LV contractility, as indicated by a higher end-systolic elastance (E_{es} , the slope of end-systolic pressure–volume relationship (ESPVR)) and VVC were observed in spermidine-treated *Atg5^{+/+}* but not *Atg5^{-/-}* mice (Fig. 3j, k, Supplementary Fig. 10e and Supplementary Table 12). Hence, spermidine-treated *Atg5^{-/-}* mice showed impaired systolic function, as indicated by a reduced ejection fraction (Fig. 3g). Collectively, these data indicate that spermidine prevents typical age-related cardiac deterioration in an autophagy-dependent manner, reducing LV hypertrophic remodeling and improving diastolic function, contractility and ventricular-vascular coupling.

Spermidine reduces blood pressure and delays progression to heart failure in *Dahl* rats

From a clinical perspective, hypertension represents one of the most important risk factors for the development of heart failure³³ and occurs in the majority of elderly patients suffering from cardiovascular disease³³. Because hypertension and a manifest heart failure phenotype are absent in physiologically aging wild-type mice¹⁴, we employed *Dahl* salt-sensitive rats fed a high-salt diet, which constitute a clinically relevant animal model of hypertension-induced hypertrophy, diastolic dysfunction and heart failure³⁴. These rats also exhibit phenotypic traits observed in hypertension-associated diseases in humans, including comorbidities such as renal dysfunction³⁵. *Dahl* salt-sensitive rats fed a high-salt diet had progressively increased mean arterial blood pressure, an effect that was delayed by 4 weeks when spermidine was co-administered with high-salt (Fig. 4a, b and Supplementary Fig. 11). Spermidine supplementation increased the plasma levels of spermidine in *Dahl* rats and led to significantly decreased plasma levels of ornithine, the substrate for the rate-limiting enzyme in polyamine biosynthesis, compared to control animals (Fig. 4c). This effect on ornithine levels may connect polyamine metabolism to the bioavailability of arginine (Supplementary Fig. 12a), the only source for the generation of the vasodilator nitric oxide (NO)³⁶, which has been shown to abrogate salt-sensitive hypertension in *Dahl* salt-sensitive rats³⁷. Therefore, the anti-hypertensive effect of spermidine might be explained by effects on arginine metabolism. Indeed, spermidine increased arginine bioavailability, as determined by an elevated global arginine bioavailability ratio (GABR, defined as arginine/[ornithine+citrulline]) (Fig. 4c), and increased the arginine/ornithine ratio, while also decreasing the cumulative level of ornithine and citrulline (Supplementary Fig. 12c, d). These findings suggest the ability of spermidine to improve NO production/bioavailability. Elevation of the GABR and the arginine/ornithine ratio, as well as decreased levels of ornithine plus citrulline (indicative of diminished arginine catabolism) have been associated with reduced cardiovascular risk^{38,39}.

To explore whether spermidine attenuates hypertension-induced hypertrophic remodeling and the progression to heart failure in this model, we assessed cardiac dimensions and

function. Spermidine treatment reduced tibia length-normalized LV mass, posterior wall thickness and heart weight, indicating that it attenuated the increase in cardiac hypertrophy observed in controls (Fig. 4d and Supplementary Table 14, 15). Furthermore, spermidine enhanced diastolic function, as reflected by a reduction in the E/E' ratio, a parameter that strongly correlates with mean LV filling pressure⁴⁰ (Fig. 4e). Indeed, LV-EDP was reduced (Fig. 4f, g) along with a reduction in LV stiffness, as reflected by a decreased myocardial stiffness constant for indexed volumes β_i (Fig. 4h, Supplementary Table 16) with a downward shift of the EDPVR (Supplementary Fig. 13) as well as an increase in the levels of total and S4080 phosphorylation of the N2B titin isoform (Supplementary Fig. 14a, b). Comparable to our findings in aging mice, enhanced diastolic function in rats was accompanied by a significant reduction of circulating TNF α levels (Supplementary Fig. 14c), a pro-inflammatory marker with increased levels in heart failure patients⁴¹.

In control animals fed a high-salt diet, relative lung and liver weights (normalized to tibia length) increased from 7 weeks of age to 14 or 19 weeks of age (Fig. 4i). Spermidine treatment significantly delayed the increases in relative lung and liver weights (Fig. 4i and Supplementary Table 15), suggesting that spermidine reduces pulmonary and systemic fluid accumulation, respectively, which are characteristic of heart failure. Ejection fraction was preserved (>70%) in all groups (Fig. 4j), implying that spermidine delays the progression from hypertension-induced hypertrophy to a phenotype that resembles heart failure with preserved ejection fraction (HFpEF). Control animals fed a high-salt diet showed higher arterial elastance (i.e. arterial stiffness) for indexed volumes (E_{a_i}), a surrogate of arterial load⁴², at 14 or 19 weeks of age, compared to 7 weeks of age. These animals appeared to compensate for this increased arterial elastance by increasing LV contractility, as indicated by an increase in end-systolic elastance for indexed volumes (E_{e_s} ; Supplementary Fig. 13b and Supplementary Table 16), leading to comparable VVC values in the control groups of different ages (Fig. 4k and Supplementary Table 16). Notably, spermidine administration decreased arterial stiffness (Supplementary Table 16), resulting in a significantly improved VVC (Fig. 4k and Supplementary Table 16), similar to the effects we observed in both young and old Atg5-competent mice treated with spermidine.

Renal abnormalities are commonly observed in chronic arterial hypertension⁴³ and contribute to the pathogenesis of heart failure in humans⁴⁴ as well as in *Dahl* rats⁴⁵, which have impaired renal salt metabolism leading to water retention and, thus, systemic volume-overload. Spermidine treatment of high-salt fed *Dahl* rats delayed the appearance of several signs of hypertensive renal injury, namely arterial hyalinosis with fibrosis, glomerulosclerosis and thrombotic microangiopathy (Fig. 4l and Supplementary Fig. 15a-c). Measurement of urinary lipocalin-2 (Lcn-2) levels, a sensitive marker of acute renal damage⁴⁶, corroborated the protective action of spermidine on renal function (Fig. 4m). Induction of autophagy by spermidine^{8,9} may contribute to renal tissue homeostasis and contribute to the anti-hypertensive effects of spermidine supplementation. Compared to control animals, spermidine-supplemented animals showed a significant increase in renal spermidine content (Supplementary Fig. 15d) and a significant decrease in the levels of SQSTM1/p62, a specific autophagy substrate whose levels decrease when autophagic flux is enhanced (Supplementary Fig. 15e). These findings suggest that autophagic processes might play a role in spermidine-induced kidney protection.

Dietary spermidine inversely correlates with cardiovascular disease in humans

Finally, we evaluated the association of dietary spermidine intake with cardiovascular diseases (including heart failure) and blood pressure in human subjects. In a prospective, population-based cohort (Bruneck Study⁴⁷), dietary intake of spermidine (as assessed by food questionnaires) was inversely associated with the risk of both fatal heart failure (a ~40% reduction in risk in the high compared to low spermidine intake groups) and clinically overt heart failure; both risks were more pronounced in men (Fig. 5a, b). Intake of spermidine was also inversely related to the risk of other cardiovascular diseases, as assessed by a composite of acute coronary artery disease, stroke and death due to vascular disease (Fig. 5c), and to systolic and diastolic blood pressures (Fig. 5d), which were significantly lower in the high compared to low spermidine intake groups. High intake of spermine or of spermine and spermidine combined showed similar associations as high intake of spermidine (Supplementary Fig. 16). In contrast, putrescine intake did not show these associations (Fig. 5a-c) and tended to be associated with an increase in blood pressure (Fig. 5d). Notably, spermidine intake showed a significant inverse association with plasma levels of soluble N-terminal pro-B type natriuretic peptide (NT-proBNP), the key clinically-used biomarker for heart failure ($r = -0.115$, $p=0.001$). Moreover, in an exploratory approach, we tested whether spermidine intake correlated with the levels of 131 plasma proteins (data not shown). This analysis revealed strong inverse associations for proteins implicated in cardiac disease, including chitinase-3-like protein 1 (CHI3L1), which is implicated in plaque inflammation, matrix degeneration, and plaque rupture ($r=-0.19$, $P=1.2\times 10^{-6}$, $FDR q=2.7\times 10^{-4}$); and growth/differentiation factor 15 (GDF-15), which is implicated in heart failure, atrial fibrillation, chronic kidney disease, and possibly vascular calcification ($r=-0.13$, $P=1.0\times 10^{-3}$, $FDR q=4.7\times 10^{-2}$).

Discussion

This study reveals that spermidine treatment in mice ameliorates hypertrophic remodeling of the aged heart, blocks age-related changes in cardiomyocyte composition and functionality, enhances diastolic function independently of effects on systemic blood pressure and extends lifespan. It thus appears plausible that lifespan prolongation by spermidine is due to suppression of death from cardiac-related causes; however, to what degree the effects of spermidine on the heart account for its lifespan prolonging effects is a highly challenging question and remains to be investigated in a suitable experimental setting. Other protective effects of spermidine (including anti-tumorigenic effects¹⁷) may also contribute to its lifespan-extending effects, although we did not detect a reduced cancer incidence in aged spermidine-treated C57BL/6 mice. Notably, unlike other longevity-promoting agents^{48,49}, spermidine had no detectable effects on glucose and insulin metabolism (Supplementary Fig. 17). Our data extend previous findings on the ability of spermidine to reduce arterial stiffness in aged mice⁵⁰.

The cardioprotective effects of spermidine may be due to several underlying mechanisms, including both direct cardiac effects as well as extracardiac (systemic and renal) effects (Fig. 6). Systemic effects by spermidine may involve anti-inflammatory processes as well as blood pressure lowering effect (in the setting of salt-induced hypertension). Both chronic

low-grade inflammation and hypertension reportedly cause mechano-elastic impairments and mitochondrial dysfunction of cardiomyocytes²⁹. Oral supplementation of spermidine promotes basal autophagic flux in cardiac tissue, and the direct protective effects of spermidine on the heart appear to require cardiomyocyte autophagy. Re-activation of basal autophagy by spermidine has recently been reported to maintain the regenerative function of skeletal muscle stem cells in aging mice⁵¹. It remains to be tested whether spermidine has a similar effect on other adult stem cells, including the putative cardiac ones that have been described to produce new and functional cardiomyocytes. Spermidine may otherwise facilitate rejuvenation of aged cardiomyocytes through increasing their mitochondria and myofilament content (as we observed in this study).

Additionally, we found that spermidine reduces salt-induced hypertension, left ventricular hypertrophy and delays the progression to heart failure in *Dahl* salt-sensitive rats. Comparable with our findings in aged mice, spermidine-fed *Dahl* rats showed increased ventricular-vascular coupling (denoting improved cardiovascular efficiency) and enhanced titin phosphorylation. A mechanistic link between spermidine and titin phosphorylation is suggested by the increased global arginine bioavailability ratio in spermidine-treated *Dahl* salt-sensitive rats. As arginine is the precursor to NO, which activates soluble guanylyl cyclase, increased arginine bioavailability should lead to increased activity of PKG, one of the main kinases that phosphorylates titin. PKG phosphorylates titin in a cardiac-specific domain (N2-Bus), and we found that spermidine treatment led to increased phosphorylation of N2-Bus both globally and at the PKG-specific residue (S4080). The functional consequence of titin phosphorylation is a reduction in titin-based myocardial passive stiffness²², possibly explaining how spermidine preserves the diastolic properties of the heart, which are disturbed in heart failure. In addition, the reduction of subclinical levels of circulating TNF α may contribute to spermidine-induced titin-phosphorylation by further increasing NO bioavailability through the reduction of oxidative stress²⁹ (Fig. 6). It remains to be elucidated whether a crosstalk between autophagy and titin phosphorylation exists.

In line with our experimental findings, epidemiological analyses corroborate the novel concept that spermidine-rich diets are preventive against cardiovascular disease and reduce the risk of cardiac death in humans. Interventional studies are warranted to test the therapeutic potential of dietary spermidine. It has to be acknowledged that estimation of dietary spermidine intake was based on food frequency questionnaires, which is the standard method in nutritional epidemiology, yet an indirect way of quantification that does not consider differences in food processing and preparation.

In summary, spermidine intake reduces cardiovascular pathologies, including hypertension and cardiac dysfunction associated with heart failure. In the aging population, the incidence and prevalence of heart failure are increasing in association with comorbidities such as obesity, diabetes and renal abnormalities. Our study paves the way for prospective clinical trials to evaluate the potential cardiovascular- and other health-promoting effects of spermidine-enriched diets.

Online Methods

Animal housing and polyamine supplementation

Wild-type C57BL/6 mice were purchased from Charles River (C57BL/6J:Crl females), Envigo, former Harlan Laboratories (C57BL/6N:Hsd females) or Janvier Labs, France (C57BL6/J:Rj males). Mice used for the *late-in-life* longevity experiments (Fig. 1d, Supplementary Tables 1, 2) were obtained from our in-house animal facility (C57BL/6J mice derived from various breeding lines were divided equally to spermidine-supplemented or control groups). These mice originated from more than 20 breeding pairs originally used for backcrossing transgenic strains. We used only wild-type mice (confirmed by PCR-based genotyping) that originated from at least five backcrosses to the C57BL/6J strain. The C57BL/6J colony established in house for backcrossing is renewed (purchased from Janvier labs) at least every 18 months to reduce genetic drift. Supplementation of polyamines (see Fig. 1a and Methods below) was conducted either *life-long* (starting at age 4 month) or *late-in-life* (starting at age 18 month). Analysis of lifespan, ‘omics’ and blood parameters, ultrastructural analyses, mitochondrial function as well as cardiac parameters (hemodynamics and echocardiography, non-invasive blood pressure measurements) were performed in independent cohorts of animals. **Cardiomyocyte-specific Atg5-deficient male mice** ($Atg5^{flox/flox}$ - $MLC2a$ - Cre^+ mice; $Atg5^{-/-}$) were generated from $Atg5^{flox/flox}$ mice (obtained from Riken BRC, Japan, with the kind consent of Dr. Noboru Mizushima)⁵² crossed with knock-in mice expressing Cre recombinase driven by the cardiomyocyte-specific α -myosin light chain ($MLC2a$ - Cre) promoter⁵³. After weaning, $Atg5^{flox/flox}$ - $MLC2a$ - Cre^+ ($Atg5^{-/-}$) and $Atg5^{flox/flox}$ - $MLC2a$ - Cre^- ($Atg5^{+/+}$, controls) mice were each randomly divided into two treatment groups (spermidine-treated and non-treated controls). Treatment was initiated in young one-month-old mice that were treated for up to 12-14 weeks of age before they were subjected to cardiac functional analyses (echocardiography and hemodynamics). This time point was selected based on a previous study⁶, showing that cardiac restricted $Atg5^{-/-}$ mice have no cardiac phenotype at 3 months of age. PCR analysis of genomic DNA from ear biopsies was performed for the assessment of genotypes using published primers “exon3-1”, “short 2” and “check 2”; *loxP*-flanked *Atg5* allele⁵² and primers “MLC2a-1”, 5'-GGATCTATGTGGAGCCCTGTCT-3' and MLC2a-2“, 5'-GCACACAAGTCCCTGGCTCTGT-3' (Cre allele)⁵³. Adult ventricular cardiomyocytes were isolated from 12-16-week-old $Atg5^{-/-}$ male mice and their age-matched control littermates using a previously reported protocol⁵⁴. Isolated cardiomyocytes were then subjected to immunoblotting of LC3, p62 and Atg5 to confirm Atg5-deficiency and impaired autophagy (see Supplementary Fig. 10). **Dahl salt-sensitive male rats** (N = 60 in total), an experimental model of hypertensive heart failure⁴⁵, were purchased at the age of 4 weeks from the Charles River Laboratories (USA). Low salt laboratory chow containing 0.3% NaCl (AIN-76A, Research Diets, Inc. USA) was fed to 60 weaning *Dahl* rats until the diet was switched to a high-salt diet (AIN-76A with 8% NaCl, Research Diets, Inc. USA) at 7 weeks of age. Twelve rats fed the low-salt diet were sacrificed at the age of 7 weeks and served as a young control group. The remaining 48 rats were randomly divided into two cohorts each consisting of two groups (N=12 animals per group): group 1 received regular drinking water without spermidine (non-treated control), whereas group 2 received regular drinking water supplemented with spermidine for a period of 7 (short-term cohort) or 12

(long-term cohort) weeks (see Fig. 4a). Blood pressure was assessed independently in the short- and long-term cohorts, with comparable results at similar ages (i.e. 7, 9, 11 weeks). Hemodynamic cardiac assessment was conducted as a terminal procedure independently in the two cohorts, yielding also comparable results with respect to spermidine effects, but at different ages (14 and 19 weeks).

Animals were housed under SPF (mice) or conventional (rats) conditions in a 12h light/dark cycle with access to food (standard chow for mice, *Ssniff*V1534) and water *ad libitum*. Autoclaved nest material and paper houses served as cage enrichment for mice. The polyamines spermidine (3 mM in all experiments, with the exception of mouse *life-long* supplementation for lifespan estimation, 0.3 mM; mouse pathology analysis, glucose tolerance test, metabolic parameters, and body composition, 0.3 and 3 mM), spermine (3 mM) and putrescine (3 mM) were administered orally via drinking water prepared from aqueous stock solutions as described elsewhere⁸ Control animals received regular drinking water. Food and water consumption was recorded twice a week at indicated ages (averaged over a time period of 4 weeks) by weighing water bottles and food pellets. Animal cages were always randomly assigned to treatment or control groups.

With the exception of animal care and housing as well as experiments performed on the 7-week-old rats cohort, the experimenters were blinded to the age and treatment of the animals. All animal experiments were performed in accordance with national and European ethical regulation (Directive 2010/63/EU) and approved by the responsible institutional (Rutgers-New Jersey Medical School's Institutional Animal Care and Use Committee) or government agencies (District Government of Upper Bavaria, Germany, and Bundesministerium für Wissenschaft, Forschung und Wirtschaft, BMWF, Austria: BMWF-66.010/0161-II/3b/2012, BMWF-66.007/0011-II/3b/2013, BMWF-66.010/0053-WF/II/3b/2014; BMWF-66.010/0160-WF/V/3b/2014, BMWF-66.007/0002-WF/V/3b/2015, BMWF-66.007/0024-WF/V/3b/2015).

Mouse lifespan analysis

For lifespan experiments, the housing group size was maintained at two or more animals per cage. This was assured by joining single-housed animals (i.e. last survivor in a cage) to other cages of the same treatment group. Regular sentinel observation was used to ascertain the SPF health status of the animals. Animals were inspected daily for their general health status. Whenever the health condition of an animal indicated that its welfare was compromised, the mouse was euthanized and classified as either (i) an *end-of-life* (EOL)¹⁶ animal likely dying within the next 24-48 hours, or (ii) a censored animal (due primarily to severe bite wounds, obvious tumors or skin lesions after excessive grooming). EOL animals were defined by established “estimation of death” criteria similar to the *Interventions Testing Program* (ITP) program guidelines of the *National Institute on Aging* (NIA)⁵⁵, with the exception that any one of these criteria was considered sufficient to indicate close natural death. The majority of animals were simply found dead during daily inspections (Supplementary Table 1). Of note, the overall lifespan observed in the present study was slightly shorter compared to other studies using C57BL/6 mice^{15,56}, a difference that may be due to differences in housing conditions, estimation-of-death criteria or the highly

stringent criteria we used to identify mice in severe discomfort, which must be euthanized, thus affecting the number of censored mice. Survival data were analyzed by Kaplan-Meier method and significant differences in survival distribution curves between the groups were determined using the Breslow test. OriginPro 2016 software (OriginLab) was used for survival data analysis, including also the calculation of lifespan estimates. Censored animals were still counted as live individuals before the time at which they were euthanized. However, during the *life-long* supplementation experiment (C57BL/6J:CrI female mice), we observed an unusually high incidence of C57BL/6-typical alopecia⁵⁷ with signs of ulcerative dermatitis early in life (between the age of 200 and 300 days), which required us to euthanize about 40% of all mice. We decided not to censor these mice, but rather to completely exclude them from the survival analysis. Notably, in this experiment, the fraction of animal loss early during the experiment was similar in the spermidine-supplemented and control groups.

Analysis of body composition and metabolic parameters in aging mice

Body composition (relative lean- and fat mass) was determined by *in vivo* NMR spectroscopy using the Minispec mq NMR analyser (Brucker Optics, USA), according to the manufacturer's instructions. General activity (assessed by the total number of beam breaks, *XT+YT counts*) as well as the respiratory exchange rate (*RER*, expressed as the volumetric quotient of carbon dioxide elimination of the animal divided by oxygen consumption, V_{CO_2}/V_{O_2}) was determined using *PhenoMaster*TM cages (TSE-Systems). Mice were singly housed and the first complete 12 hour dark- and light-cycles were recorded for parameter analysis after an initial adaptation phase of 8 hours.

Intraperitoneal glucose tolerance test

Intraperitoneal glucose tolerance tests were performed as previously described⁵⁸. Briefly, the food was removed for 16 to 18 hours overnight. During the experiment, mice were singly housed in empty cages without food, water or bedding. The basal fasting blood glucose level was determined using a drop of blood collected from the tail vein, using an Accu-Chek Aviva glucose analyzer (Roche/Mannheim). Thereafter mice were injected intraperitoneally with 2 g of glucose/kg fasting body mass and blood glucose levels were determined 15, 30, 60 and 120 minutes after glucose injection.

Fasting insulin determination

Fasting insulin was measured in plasma obtained from 3 hour fasted mice (water supplied *ad libitum*) using an ultra-sensitive mouse insulin ELISA Kit (Crystal Chem, Downers Grove, Illinois, USA). The wide range assay protocol was performed according to the manufacturer's protocol. Insulin concentrations of the samples were calculated using a semi-logarithmic 4-parameter fit standard curve in Prism 6 (GraphPad Software Inc, La Jolla, California, USA).

Non-invasive blood pressure measurements

Systolic, mean and diastolic blood pressures, as well as heart rate, were non-invasively measured in conscious animals by the tail-cuff method using the CODATM system (Kent

Scientific Corporation, USA). Animals were placed in a cylindrical holder on a temperature-controlled platform (kept at 37 °C) and recordings were performed in steady-state conditions. Blood pressure values were averaged from three consecutive measurements.

Echocardiography

Transthoracic echocardiography was performed similarly as described⁵⁹. Briefly, lightly anaesthetized mice (0.5% isoflurane and 99.5% O₂) and rats (2% isoflurane and 98% O₂) were placed on a temperature-controlled warming pad (kept at 37 °C) and imaged in the supine position using a high-resolution micro-imaging system equipped with a 30-Mhz and 17.5-Mhz linear array transducer (Vevo770™ Imaging System, VisualSonics Inc., Canada), respectively. Parasternal long-axis M-mode tracings of the left ventricle (LV) were recorded at the level just above the papillary muscles and LV end-diastolic diameter (LVEDD), LV end-systolic diameter (LVESD), interventricular septum thickness (IVS) and LV posterior wall thickness (PW) were measured. Fractional shortening was calculated using the equation: $100 \times [(LVEDD - LVESD) / LVEDD]$. Left ventricular end-systolic and end-diastolic volumes as well as ejection fraction were calculated according to the Teichholtz formula and the LV mass was calculated according to the Troy formula⁶⁰. The ratio of peak early filling velocity of transmitral flow (E) to the corresponding mitral valve annulus velocity (E') was evaluated using pulsed-wave and tissue Doppler imaging, respectively. All measures were averaged from three consecutive cardiac cycles under stable conditions.

Hemodynamic pressure-volume measurements

Invasive hemodynamic measurements and analysis of pressure-volume (PV) loops were performed as a terminal procedure according to established protocols⁶¹. Mice and rats were anaesthetized (induction: 3-4% isoflurane with 96-97% O₂; maintenance: 1-2% isoflurane with 98-99% O₂), intubated and mechanically ventilated (rats, SAR 1000, CWE, Inc.; mice, Harvard Mini-Vent (type 845), Harvard Apparatus). The animals were placed on a temperature-controlled heating platform (TC-1000, CWE, Inc.) and their core temperature was maintained at 37.5 °C. Heart rate (HR) was continuously monitored using an electrocardiogram (Animal Bio Amp, FE136; ADInstruments). A mouse 1.4 F or rat 2.0 F pressure-conductance catheter (SPR-839 and SPR-838, respectively; Millar instruments) was inserted into the right carotid artery and advanced into the ascending aorta. After recording aortic (systemic) blood pressure, the catheter was advanced through the aortic valve into the LV where PV signals were continuously obtained (MPVS ultra, Millar Instruments) and recorded in a digital-form (MPVS PL3508 PowerLab 8/35, ADInstruments) at the acquisition rate of 2 kHz for later offline analysis (LabChart 8 pro, ADInstruments). Animals were allowed to stabilize for 5 minutes, then baseline load-dependent parameters of systolic and diastolic function, including LV end-systolic pressure (ESP), LV end-diastolic pressure (EDP), LV end-systolic volume (ESV), LV end-diastolic volume (EDV), stroke volume (SV), cardiac output (CO), arterial elastance (E_a), ejection fraction (EF), maximal slope of LV systolic pressure increment (dp/dt_{max}), maximal slope of diastolic pressure decrement (dp/dt_{min}) and time constant of LV pressure decay (τ) were measured and averaged from 10 consecutive beats, with ventilation suspended at end-expiration. After baseline measurements, transient occlusion of the inferior *vena cava* (again with ventilation suspended) was performed and used to calculate multibeat-derived load-independent

measures of cardiac systolic and diastolic functions: linear end-systolic pressure-volume relationship (ESPVR), calculated as $ESP = \text{end-systolic elastance (Ees)} * ESV + V_0$, was used for the evaluation of cardiac contractility, while exponential end-diastolic pressure-volume relationship (EDPVR), calculated as $EDP = \alpha * \exp^{\beta * EDV}$, was implemented in assessing end-diastolic stiffness. In addition, ventricular-vascular coupling (VVC), indicative of cardiovascular efficiency, was calculated as the ratio between Ees and Ea. To correct for the large differences in body (and heart) size between young (7-week-old) and older (14- and 19-week-old) *Dahl* salt-sensitive rats, volumes were indexed to body surface area⁶³ as defined by $9.1 \times (\text{body weight})^{2/3}$. A polyethylene catheter was inserted into the right external jugular vein for hypertonic saline (10% NaCl) injection (10 μ l in mice and 40 μ l in rats) to calculate parallel conductance at the end of the experiment. Due to detected discrepancies of conductance- and echocardiography-derived left ventricular (LV) volumes in *Atg5*-deficient mice (not shown), the slope factor α (a factor that is used to correct conductance-based estimation of ventricular volumes) was calculated using echocardiography-derived stroke volume, which correlates with the gold-standard method of volume estimation using Doppler flow-probes⁶². After assessment of hemodynamic parameters, animals were sacrificed and a gravimetric analysis of different organs, including heart, lungs, liver, spleen and kidneys, was performed.

Histological evaluation

Tissues were fixed in 4% neutral-buffered formaldehyde and paraffin-embedded. Kidneys were cut into 4 μ m thick sections followed by periodic acid-Schiff (PAS) staining (Merck, Darmstadt, Germany). The extent of glomerular injury was evaluated by assigning a semiquantitative PAS score as described previously⁶⁴. Furthermore, we evaluated the extent of arterial hyalinosis and fibrosis semiquantitatively using a similar scoring system as above. The number of tubular casts in 6 adjacent high-power fields (magnification 400x) was counted. To assess the extent of renal fibrosis and damage, picrosirius red staining was performed. Renal tissue was first stained with Gill's hematoxylin (Merck), then with 1% Sirius red (Sigma-Aldrich, St. Louis, MO, USA) in a saturated aqueous solution of picric acid and then differentiated in acidified water. To investigate the cardiac death and cancer development phenotype (pathology analysis), 4 μ m thick sections of heart, liver, brain, spleen and kidney were stained with hematoxylin/eosin stain as follows: after rehydration, sections were stained in Mayers' acid hemalum for 2 min, blued in tap water for 2 min, contrasted with Eosin Y for 15 sec, rinsed in tap water for 5 sec, dehydrated in an increasing ethanol series and placed in xylene before mounting with Entellan® (all chemicals from Merck, Germany). Slides were read using an Axioplan® brightfield microscope (Zeiss, Germany) by two pathologists independently (D.J., F.N.).

Assessment of urinary Lcn-2 levels

Urinary levels of Lcn-2 protein were assessed using the Rat Lcn-2/NGAL DuoSet (R&D Systems, Abingdon, UK) kit according to the manufacturer's instructions.

Transcriptome expression profiling

Expression profiling was done from hearts of four treated (3 mM *life-long* spermidine supplemented, see Fig. 1a) and four untreated mice at the age of 30-32 months, as well as

from four six months old untreated control mice. Mice were sacrificed between 9 and 12 p.m. (noon). Hearts were dissected, immediately frozen in liquid nitrogen and stored at -80 °C. For total RNA isolation using RNeasy Midi kits (Qiagen), hearts were thawed in Trizol Reagent (Sigma) and homogenized using a Polytron homogenizer (Heidolph). 500 ng of total RNA was amplified in a single round using the Illumina TotalPrep RNA Amplification Kit (Ambion). 750 ng of amplified RNA was hybridized to Illumina MouseRef8 v2.0 Expression Bead Arrays covering 25,600 annotated RefSeq transcripts. Staining and scanning (Illumina HiScan Array reader) were done according to the Illumina expression protocol. Illumina Genomestudio software was used for background correction and normalization (cubic spline algorithm). Significant gene regulation was analysed using SAM (Significant Analysis of Microarrays) included in the TM4 software package⁶⁵. False discovery rates (FDRs) were calculated by 1000 random permutations. The selection of the top differentially expressed genes with reproducible up- or down-regulation includes genes with an FDR below 10% and a mean fold change above 1.5 fold. Over-represented functional annotations (Gene Ontology) were identified using the Ingenuity Pathway Analysis. Genes and samples were clustered for heat map representation using the hierarchical clustering function (complete linkage) of Genesis software (release 1.7.6)⁶⁶.

Proteomics analysis

Heart specimens were obtained from three aged, three young and three aged mice treated with spermidine. Whole tissue lysates (50 mM Tris-HCl, pH 7.4, 1 mM EDTA, 1 mM EGTA, 1% Triton X-100 supplemented with 1x *Complete*[®] protease inhibitor cocktail (Roche)) were prepared in SDS loading buffer, samples were reduced with 1 mM DTT (Sigma-Aldrich) for 5 min at 95 °C and alkylated using 5.5 mM iodoacetamide (Sigma-Aldrich) for 30 min at 20 °C. Protein mixtures were separated by 4-12% gradient SDS-PAGE (NuPAGE, Invitrogen). The gel lanes were cut into 6 equal slices, the proteins were in-gel digested with trypsin (Promega)⁶⁷, and the resulting peptide mixtures were processed on STAGE tips⁶⁸ and analyzed by LC-MS/MS. Mass spectrometric (MS) measurements were performed on an LTQ Orbitrap XL mass spectrometer (Thermo Fisher Scientific) coupled to an Agilent 1200 nanoflow-HPLC (Agilent Technologies GmbH, Waldbronn, Germany) as described⁶⁹. MS raw data files were uploaded into MaxQuant software (version 1.4.1.2 (ref. 70)), which was used for identification of proteins and protein ratio assignment for peak detection, generation of peak lists of mass error corrected peptides and for database searches. A full-length UniProt mouse database additionally containing common contaminants such as keratins and enzymes used for in-gel digestion (based on UniProt mouse FASTA version July 2014) was used as a reference.

Carbamidomethylcysteine was set as a fixed modification; methionine oxidation and protein amino-terminal acetylation were set as variable modifications and label-free was chosen as the quantitation mode. Three miscleavages were allowed, enzyme specificity was trypsin/P, and the MS/MS tolerance was set to 0.5 Da. The average mass precision of identified peptides was in general less than 1 ppm after recalibration. Peptide lists were further used by MaxQuant to identify and relatively quantify (label-free quantification, LFQ) proteins using the following parameters: peptide and protein false discovery rates, based on a forward-reverse database, were set to 0.01; the minimum peptide length was set to 7; the minimum number of peptides for identification and quantitation of proteins was set to two, of which

one must be unique; the minimum ratio count was set to two; and identified proteins were requantified. The 'match-between-run' option (1 min) was used. The 10% most reproducible changes based on TTEST analysis between aged control and aged spermidine groups (yielding a p-value cut-off $p < 0.15$) were considered as potential *hits*. To visualise age- or spermidine-induced changes in protein abundance (*heat map presentation*), the LFQ protein intensities of each sample were divided by the mean of respective aged control intensities (LFQ *Ratios*). Proteins and samples were clustered for heat map representation using the hierarchical clustering function (complete linkage) of Genesis software (release 1.7.6)66.

Metabolite analysis by high performance liquid chromatography (HPLC) and mass spectrometry (MS)

Tissue metabolite analysis was performed on whole tissue lysates. Tissues were snap frozen in liquid nitrogen and stored at $-80\text{ }^{\circ}\text{C}$ until metabolite extraction. For metabolite extraction, tissues were pulverized on dry ice using mortar and pestle. A quantitative HPLC-MS/MS-based determination of polyamines (ornithine, putrescine, spermidine and spermine) was performed essentially as described⁷¹ in plasma or from whole blood and cardiac tissue acid extracts as indicated. Plasma was prepared by centrifugation of EDTA-collected blood at 2,500 g for 20 min. 10 μl EDTA-collected blood or 10-15 mg pulverized tissue was used to generate whole blood- or tissue-extracts, respectively, with a final extract volume of 750 μl .

For metabolomic analysis, mice (12 animals per group) were fasted overnight (12-16 hours) and hearts were removed and snap frozen (liquid nitrogen) immediately after sacrificing the animals. Cardiac tissue extracts using 20-40 mg tissue wet weight were prepared by cold-methanol extraction as described⁷². A boiling ethanol extract from yeast grown aerobically on ^{13}C -glucose as the carbon source served as an internal standard for MS analysis⁷³ and was spiked into tissue samples before extraction. Metabolomics samples were measured with a LC/MS system from Thermo Fisher Scientific™. A Dionex Ultimate 3000 HPLC setup equipped with an Atlantis T3 C18 pre- and analytical column (Waters, USA) was used for compound separation prior to mass spectrometric detection with an Exactive™ Orbitrap system. The method was adapted from *Buescher et al.*⁷⁴. The injection volume was 10 μL per sample and negative ionization of metabolites was carried out via heated electrospray ionization. For the online detection of the metabolites a full scan of all masses between 70 and 1,100 m/z with a resolution of 50,000 (at m/z 200) was used. LC/MS-data acquisition was conducted with Xcalibur software (version 2.2 SP1, Thermo Fisher Scientific (Waltham, USA)), automated peak integration with TraceFinder™ software (version 3.2, Thermo Fisher Scientific (Waltham, USA)). Screening and manual correction of peak integrations were done within the TraceFinder™ package. ^{12}C -peak area/ ^{13}C -peak area ratios were normalized to the respective tissue sample wet weight. Age- or spermidine-induced changes in metabolite abundance were identified by dividing ^{12}C -peak area/ ^{13}C -peak area ratios of each sample to the mean of respective aged control samples (Aged control-normalized *Ratios*) and the median was used for *heat map* representation. Principal Component Analysis (PCA) was applied to the complete dataset using the R-function *prcomp* (stats-package) with R version 3.1.1 in order to detect potential clustering and distances between samples.

Plasma arginine and citrulline determination

Arginine and citrulline concentrations were measured in serum with modifications of previously described chromatographic methods^{75,76}. Briefly, after precipitation of serum with perchloric acid following neutralization of the supernatant with sodium carbonate, the extracted amino acids were derivatized online with o-phthalaldehyde and separated on a reverse phase column with gradient elution. Quantification was performed with ratios of fluorescence signals of the relevant amino acids to the internal standard norvaline in comparison to the appropriate calibration curves. Intra-assay and inter-assay CV's were all below 10%.

Isolation of cardiac mitochondria and high-resolution respirometry

Isolation of cardiac mitochondria and high-resolution respirometry was performed similarly to published methods²⁶, using an isolation buffer containing 0.2% BSA and 5 mg/ml bacterial protease (Sigma-Aldrich, P8038). Hearts were quickly excised immediately after terminal blood collection under isoflurane anaesthesia and processed as described²⁶. Optical density at 600 nm (OD₆₀₀) of the final mitochondrial suspension (isolation buffer including BSA, but excluding protease) was determined by serial dilutions in a TECAN GeniusPro plate reader and served as an estimate of mitochondrial mass used for normalization. Oxygen consumption was assayed at 37 °C with an Oxygraph-2k high-resolution respirometer (Oroboros Instruments, Austria) according to the manufacturer's recommendations. OD₆₀₀ equivalents of isolated myocardial mitochondria corresponding to 10-20 µg mitochondrial protein were diluted in 2 ml equilibrated measurement medium (100 mM sucrose, 20 mM K⁺-TES (pH=7.2), 50 mM KCl, 2 mM MgCl₂, 1 mM EDTA, 4 mM KH₂PO₄, 3 mM malate and 0.1% (v/v) BSA) within a closed and calibrated system with constant stirring. For measurement of complex I activity, 5 mM pyruvate and 10 mM glutamate were added as reduced substrates after initially recording residual oxygen consumption (*ROX*) resulting in leak respiration (*LEAK*), followed by sequential additions of 450 µM ADP (*OXPHOS*) and 10 µM cytochrome c (*OXPHOS + CytC*). 1.25 µM oligomycin were finally used to monitor the residual respiration (proton leak) followed by titration with FCCP (0.5 µM steps) to assess maximum respiration in uncoupled state and subsequent inhibition of respiratory activity through antimycin A. For each oxygraphic protocol (see Supplementary Fig. 7a), two mice were always processed in pairs (one aged control (24M) combined with either one aged spermidine-supplemented (24M+S) or one young control (5M)). The absolute oxygen concentration remained above 100 nmol/ml throughout all recordings.

Plasma cytokine determination

Plasma cytokine levels of apparently healthy mice or rats (i.e. subclinical cytokine levels) were assessed by electrochemiluminescence-based immunoassays using the MSD V-Plex Plus Proinflammatory Panel 1 (mouse) assay kit or a customized TNF α / IL-10 V-Plex Rat cytokine kit (Meso Scale Diagnostics, USA). 25 µl of plasma derived from EDTA-collected whole blood by centrifugation (20 min, 2500 g) was processed according to the manufacturer's instructions. Whole blood was obtained from isoflurane-anesthetized animals at the age of 21 (non-fasted) or 23 (overnight-fasted before sacrifice) months by

terminal bleeding (mice) or directly from the heart immediately at the end of hemodynamic assessment (rats). In addition to analyzing the complete inflammatory cytokine dataset (subclinical inflammatory status) of aged mice (Supplementary Fig. 8a), we performed an additional analysis, in which mice with *potentially* acute inflammatory conditions were excluded (Supplementary Fig. 8b), due to the fact that such mice, though lacking overt clinical manifestations, may strongly confound interpretation of the age-associated (chronic) low-grade inflammation status. Animals with two or more statistically-identified outlier cytokines were considered as animals with an acute inflammatory condition. Animals with a single outlier cytokine were included in the analysis, but the respective value was winsorized (see Supplementary Fig. 8). An outlier cytokine was identified using the 2.2-fold inter-quartile range (IQR) labeling rule applied to the respective group. Of note, the total number of excluded and winsorized values was similar in all aged groups.

Immunoblotting and assessment of autophagic flux

Measurements of the protein levels of APG5L/ATG5 and the autophagy-substrate p62/SQSTM1, as well as measurements of LC3 lipidation (LC3-II/GAPDH ratio), were performed on tissue extracts using lysis buffer containing 50 mM Tris-HCl, pH 7.4, 1 mM EDTA, 1 mM EGTA, 1% Triton X-100 supplemented with 1x *Complete*[®] protease inhibitor cocktail (Roche). Immunoblotting on polyvinylidene difluoride (PVDF) membranes was performed by standard procedures and probed with antibodies recognizing APG5L (ATG5) (dilution: 1:1000, ab018327, Abcam), p62 (SQSTM1) (dilution: 1:1000, PM045, MBL), LC3B (dilution: 1:1000, #2775, Cell Signaling Technologies), GAPDH (dilution: 1:1000, #2118, Cell Signaling Technologies), and horseradish peroxidase (HRP)-linked anti-rabbit IgG (dilution: 1:3000, #7074, Cell Signaling Technologies). Data were analyzed and quantified by densitometry with ImageLab software (Bio-Rad laboratories). Full scans of representative blots are shown in Supplementary Fig. 18. Autophagic flux in wild-type animals was assessed using leupeptin-based inhibition of LC3-II turnover according to a published protocol³⁰. Following 4 weeks spermidine supplementation, 13-month-old C57BL6/JRj male mice (Janvier, France) were subjected to intraperitoneal (i.p.) injection of leupeptin (40 mg/kg body weight, Sigma, Austria) or vehicle (0.9% sterile sodium chloride solution). Fifty minutes after the i.p. injection, animals were sacrificed and hearts were excised. Age-matched mice that did not receive spermidine were used as controls. Cardiac tissues were subjected to immunoblot analysis of LC3 (see above).

Autophagic flux using transgenic animals

Transgenic mice with cardiac-specific expression of tandem-fluorescent mRFP-GFP-LC3 (Tg-tf-LC3) generated on a C57/BL6 background with the mouse α -Myosin Heavy Chain promoter were used³¹. In order to evaluate autophagic flux *in vivo*, 3-month-old Tg-tf-LC3 mice were supplemented with 3 mM spermidine for 2 weeks (mice receiving normal drinking water served as controls). In some mice, chloroquine (10 mg/kg) was injected 4 hours before euthanasia and the number of fluorescent LC3 dots (indicative of autophagosomes and autolysosomes) was determined by confocal microscopy. Fresh heart slices were embedded with tissue-TEK OCT compound (Sakura Finetechnical Co., Ltd.) and frozen at -80 °C. Sections 10 μ m in thickness were obtained from the frozen tissue samples using the Leica Biosystems CM3050 S Research Cryostat (Leica), air-dried for 30 min, fixed

with 10% formalin for 10 min, mounted using a reagent containing DAPI, and viewed under a fluorescence microscope.

Mitophagy evaluation

Evaluation of mitochondrial autophagy was achieved by monitoring Mito-Keima and Lamp1–YFP fluorescence as previously described³². Briefly, 6-month-old (young) and 18-month-old (aged) C57BL/6J mice were injected with AAV-Mito-Keima⁷⁷ and AAV9-Lamp1–YFP⁷⁷ 4 weeks preceding analyses of Mito-Keima fluorescence and Lamp1–YFP fluorescence using confocal microscopy. Mice were treated with spermidine (3 mM) or vehicle (normal drinking water) for 3 weeks. Ratiometric images of Mito-Keima fluorescence (561 nm/457 nm excitation) were calculated and visualized in blue color. High ratiometric signals were defined as Mito-Keima positive areas, indicating mitochondrial autophagy (mitophagy). Mito-Keima fluorescence detected after excitation at 561 nm is shown in red color, while fluorescence after excitation at 457 nm is shown in green color. Merged images of Mito-Keima fluorescence (after 561 nm excitation) and Lamp1–YFP (shown in blue color) confirmed lysosomal localization of Mito-Keima-positive areas.

Titin isoform separation and phosphorylation assays

Homogenized myocardial samples were analyzed by 1.8% SDS–PAGE. Protein bands were visualized using Coomassie blue, scanned, and measured densitometrically, as described⁷⁸. In place of a protein size marker in the titin range, human heart and diaphragm extracts (Source: Biobank at Dept. of Cardiovascular Physiology, Bochum, Germany) were used as *standards* for N2B/N2BA and N2A isoforms identification⁷⁹, respectively. Western blotting was performed using anti-phosphoserine/threonine antibodies (Cat. No. PP2551, Biotrend Chemicals, Cologne, Germany, former ECM Biosciences) to measure global titin phosphorylation, and with affinity-purified phosphosite-specific anti-titin antibodies against phospho-S4080 in the N2Bus domain of mouse titin (custom-made against the peptide LFS(PO3H2)EWLRNI; dilution 1:500; Eurogentec, Brussels, Belgium)⁷⁹. As a secondary antibody, we used horseradish peroxidase-conjugated IgG (Acris Antibodies, Herford, Germany). For signal amplification we used the Enhanced Chemoluminescence Western blot detection kit (GE Healthcare, Little Chalfont, UK). Staining was visualized using the LAS-4000 Image Reader (Fuji Science Imaging Systems), and densitometry was performed using Quantity One 1-D Analysis software (Bio-Rad laboratories). Equal protein loading and transfer was confirmed by densitometry of the signal on Coomassie-stained polyvinylidene fluoride (PVDF) membranes and western blot signals were normalized to the corresponding PVDF signals. Full scans of representative blots are shown in Supplementary Fig. 18. Two samples per group were processed in parallel on the same blot and the *standards* (always using the same identical extracts) were used for intra-gel normalization, allowing for quantitative inter-gel comparisons.

Design-based stereology

Mouse hearts were fixed by vascular perfusion with 4% neutral buffered formaldehyde and kept in the fixative for at least 24 h. Then the left ventricle (including the interventricular septum) was isolated, weighed and randomly sampled for electron microscopy (EM). The samples were post-incubated in a fixative containing 1.5% paraformaldehyde and 1.5%

glutaraldehyde in 0.15 M HEPES buffer. Subsequently, the samples were post-fixed with 1% osmium tetroxide, stained *en bloc* with a half-saturated uranyl acetate/water solution, dehydrated in an ascending acetone series and finally embedded in epoxy resin. From the embedded samples, ultrathin sections were generated, mounted on EM support grids and post-stained with lead citrate and uranyl acetate. The sections were analysed with a Morgagni transmission electron microscope (FEI, Eindhoven, Netherlands) and test fields for morphometry were assessed using a digital camera according to a systematic uniform random sampling scheme⁸⁰. To estimate the volume fractions of cardiomyocytes and their organelles (myofibrils, mitochondria, sarcoplasm, nuclei, lipofuscin granules) as well as interstitium and its subcompartments (collagen fibrils, capillaries), point grids were projected onto the test fields and the number of points hitting the structures of interest and the reference volume were counted. The volume fraction of a structure was calculated by dividing the number of points hitting the structure by the number of points hitting the reference volume⁸¹. The total volume was then calculated by multiplying the volume fraction of a structure with the reference volume, e.g. the volume of the left ventricle. The latter was estimated by dividing the ventricular weight by the density of muscle tissue, 1.06 g/cm³ (ref. 82).

Human study subjects, quantification of nutritional intakes and data analyses

Study subjects belonged to the Bruneck Study, a prospective, population-based survey on the epidemiology and pathogenesis of atherosclerosis and cardiovascular disease (CVD)⁴⁷. Extended study details and risk factor assessment using validated standard procedures can be found online in the Supplementary Note (Section on *Information on Human Data Analysis*). Long-term average dietary intakes were ascertained by a dietitian-administered 118-item food frequency questionnaire (FFQ). This questionnaire was based on the gold standard FFQ by Willett and Stampfer⁸³ and modified to better fit the dietary peculiarities in the survey area. Special nutrient data were compiled for polyamines using published data (see online Table at the *Supplementary Information on Human Data Analysis*). **Death due to heart failure** was defined according to the *International Statistical Classification of Diseases and Related Health Problems, 10th revision (ICD-10)* diagnosis codes I50.x, I13.0, I13.2, I11.00, I11.01 and I97.1 (considering heart failure following cardiac surgery or due to presence of cardiac prosthesis). **Clinically overt heart failure** was defined according to gold standard Framingham criteria (presence of at least 2 major criteria or 1 major criterion in conjunction with 2 minor criteria)⁸⁴ and assessed as part of the 2010 re-examination of the Bruneck Cohort. The primary composite CVD (**incident CVD**) endpoint included vascular death (from myocardial infarction [MI], ischemic stroke, or sudden cardiac death), acute coronary artery disease (consisting of nonfatal MI, new-onset unstable angina defined as angina at rest, crescendo angina or new-onset severe angina, and acute coronary interventions), and ischemic stroke. MI was defined by the World Health Organization's criteria for definite disease status. Stroke was classified according to the criteria of the National Survey of Stroke. All other revascularization procedures (percutaneous intervention, bypass, and surgery) were carefully recorded. Ascertainment of events or procedures did not rely on hospital discharge codes or the patient's self-report but rather on a careful review of medical records provided by the general practitioners and files of the Bruneck Hospital and the extensive clinical and laboratory examinations performed as part of the study protocols.

Incident CVD events were ascertained from 1995 through 2010, and 100% follow-up was achieved⁸⁵. Causes of death as well as clinically overt heart failure were categorized by a senior researcher who was unaware of the dietary data. Dietary intakes were cumulatively averaged over follow-up visits to capture long-term dietary behaviour and to reduce within-subject variability. Polyamine intake was log-transformed and adjusted for total caloric intake by using the residual method⁸⁶ in a log-log simple linear model. Polyamine intake was then scaled to unit variance such that effects were estimated for a one-standard deviation increase in intake.

Plasma protein levels were measured by the Olink Proseek Multiplex Inflammation I (n=92 proteins) and Olink Proseek Multiplex CVD I (n=92 proteins) proximity extension assays⁸⁷ in samples from participants of the Bruneck 2000 assessment (n=658). For proteins measured in both assays (n=23 proteins), measurements from the newer Inflammation I assay were used, and proteins with more than 25% non-detects (n=30) were excluded, leaving 131 proteins for analysis. Proteins with skewness exceeding 1 were log-transformed. Skewness was calculated using the `e1071` package for R, which used a formula m_3/s^3 , where m_3 is $\sum_i (x_i - \mu)^3/n$, μ the sample mean, n the sample size, s the sample standard deviation, and x_i the individual data values. Polyamine intake was averaged over the assessments made in 1995 and 2000, calorie-adjusted and log-transformed. Association of dietary polyamine intake to the plasma protein levels was tested using Pearson correlation partial to age, sex, and caloric intake, and in this analysis multiple testing was accounted for by the Benjamini-Hochberg procedure (particularly suitable for high-dimensional data).

The numbers of unique subjects and of diet records used for this analysis were 829 and 2540, respectively. Statistical procedures are detailed in the Supplementary Note. All P values are two-sided and an α level of 0.05 is used throughout. Analyses were conducted with R 3.1.1. See *Supplementary Note on Human Data Analysis* for more details on outcome and methodologies.

Statistical analysis of the experimental data

Data are presented either as dot-plots and line graphs showing mean \pm s.e.m., or as box-plots, showing mean (dot), median (center line) and interquartile range (IQR), along with whiskers showing minima and maxima within 1.5 or 2.2 IQR as indicated. Sample sizes were chosen based on literature (i.e. lifespan analyses⁵⁵) or using standard power analysis (statistical power: 0.8 and α value: < 0.05) based on our preliminary echocardiographic data obtained from young and aged animals yielding 9 or 12 animals per group (Student's *t*-test or ANOVA, respectively). For some measurements in mice, sample size was adapted to the observed effect size and numbers increased to 15-20 animals per group. Indicated sample size (see figure legends) always refers to biological replicates (independent animals). If not otherwise stated, statistical testing was performed using IBM SPSS statistics software (Version 23). Student's *t*-test (paired or unpaired, as appropriate) and analysis of variance (ANOVA) with Tukey's post-hoc tests were used for comparisons between two or multiple groups, respectively. Where appropriate, a two-way ANOVA was applied (independent or mixed design that was Greenhouse-Geisser-corrected in case of sphericity violation as tested by Mauchly's test) followed by testing simple main effects (i.e. multiple comparisons of

different levels of each factor that were Bonferroni-corrected if the factor had more than 2 levels) in case of main factor⁸⁸ or interaction significance. Myocardial chamber stiffness constant (β) and end-systolic elastance (Ees) were compared between the groups including other parameters in the fitting equation (α in case of exponential end-diastolic pressure-volume relationship and V_0 in case of linear end-systolic pressure-volume relationship) as co-variates to account for their influence using analysis of co-variance (ANCOVA)⁸⁹ after confirming homogeneity of regression slopes between the compared groups.

The reported significance values are always two-sided. Overall normal distribution of data (residuals) was confirmed using Shapiro-Wilk's test. Homogeneity of variance was tested using Levene's test. Data violating these assumptions were transformed to meet the assumptions or tested as follows: non-normally distributed data were tested by non-parametric Kruskal-Wallis test after confirming equality of ranks variances (tested by non-parametric Levene's test) and followed by multiple comparisons using Mann-Whitney *U* test controlling for family-wise error rate by adjusting the significance level (α) according to the number of multiple comparisons (n) ($\alpha=0.05/n$). Whenever heterogeneous variances were an issue, Welch's *t*-test or Welch's test with *Games-Howell*-corrected post-hoc comparisons were applied.

To compare tumor incidence in aged mice, binomial logistic regression was conducted. Details of statistical analysis applied to *Human* data, *Omics* data or lifespan analyses by Kaplan-Meier method are indicated in their respective sections in the *Methods*.

Supplementary Material

Refer to Web version on PubMed Central for supplementary material.

Authors

Tobias Eisenberg^{1,2,*}, Mahmoud Abdellatif^{3,*}, Sabrina Schroeder¹, Uwe Primessnig^{3,4}, Slaven Stekovic¹, Tobias Pendl¹, Alexandra Harger^{1,5}, Julia Schipke^{6,7}, Andreas Zimmermann¹, Albrecht Schmidt³, Mingming Tong⁸, Christoph Ruckenstuhl¹, Christopher Dammbroeck¹, Angelina S. Gross¹, Viktoria Herbst³, Christoph Magnes⁹, Gert Trausinger⁹, Sophie Narath⁹, Andreas Meinitzer¹⁰, Zehan Hu^{11,12}, Alexander Kirsch¹³, Kathrin Eller¹³, Didac-Carmona Gutierrez¹, Sabrina Büttner^{1,14}, Federico Pietrocola^{15,16,17,18,19}, Oskar Knittelfelder¹, Emilie Schrepfer^{30,31}, Patrick Rockenfeller^{1,20}, Corinna Simonini³, Alexandros Rahn⁶, Marion Horsch²¹, Kristin Moreth²¹, Johannes Beckers^{21,22,23}, Helmut Fuchs²¹, Valerie Gailus-Durner²¹, Frauke Neff^{21,24}, Dirk Janik^{21,24}, Birgit Rathkolb^{21,23,25}, Jan Rozman^{21,23}, Martin Hrabe de Angelis^{21,22,23}, Tarek Moustafa^{1,5}, Guenter Haemmerle¹, Manuel Mayr²⁶, Peter Willeit^{27,28}, Marion von Frieling-Salewsky²⁹, Burkert Pieske^{3,4,36}, Luca Scorrano^{30,31}, Thomas Pieber^{5,9}, Raimund Pechlaner²⁷, Johann Willeit²⁷, Stephan J. Sigrist^{32,33}, Wolfgang A. Linke²⁹, Christian Mühlfeld^{6,7}, Junichi Sadoshima⁸, Joern Dengjel^{11,12}, Stefan Kiechl²⁷, Guido Kroemer^{15,16,17,18,19,34,35,#}, Simon Sedej^{2,3,#}, and Frank Madeo^{1,2,#}

Affiliations

¹Institute of Molecular Biosciences, NAWI Graz, University of Graz, Graz, Austria
²BioTechMed Graz, Graz, Austria ³Department of Cardiology, Medical University of Graz, Graz, Austria ⁴Department of Internal Medicine and Cardiology, Campus Virchow-Klinikum, Charité – University Medicine Berlin, Berlin, Germany
⁵Department of Internal Medicine, Medical University of Graz, Graz, Austria
⁶Institute of Functional and Applied Anatomy, Hannover Medical School, Hannover, Germany ⁷Cluster of Excellence REBIRTH (From Regenerative Biology to Reconstructive Therapy), Hannover, Germany ⁸Department of Cell Biology and Molecular Medicine, Rutgers-New Jersey Medical School, Newark, USA ⁹Joanneum Research Forschungsgesellschaft m.b.H., HEALTH, Institute for Biomedicine and Health Sciences, Graz, Austria ¹⁰Clinical Institute of Medical and Chemical Laboratory Diagnostics, Medical University of Graz, Graz, Austria ¹¹FRIAS Freiburg Institute for Advanced Studies, Department of Dermatology, Medical Center, ZBSA Center for Biological Systems Analysis, BIOS Centre for Biological Signalling Studies, University of Freiburg, Freiburg, Germany ¹²Department of Biology, University of Fribourg, Fribourg, Switzerland ¹³Clinical division of Nephrology, Medical University of Graz, Graz, Austria ¹⁴Department of Molecular Biosciences, The Wenner-Gren Institute, Stockholm University, Stockholm, Sweden ¹⁵Equipe 11 labellisée Ligue contre le Cancer, Centre de Recherche des Cordeliers, Paris, France ¹⁶Cell Biology and Metabolomics platforms, Gustave Roussy Comprehensive Cancer Center, Villejuif, France ¹⁷INSERM, U1138, Paris, France ¹⁸Université Paris Descartes, Sorbonne Paris Cité, Paris, France ¹⁹Université Pierre et Marie Curie, Paris, France ²⁰Kent Fungal Group, School of Biosciences, University of Kent, Canterbury, Kent, UK ²¹German Mouse Clinic, Institute of Experimental Genetics, Helmholtz Zentrum München, German Research Center for Environmental Health, Neuherberg, Germany ²²Chair of Experimental Genetics, School of Life Science Weihenstephan, Technische Universität München, Freising, Germany ²³German Center for Diabetes Research (DZD), Neuherberg, Germany ²⁴Institute of Pathology, Helmholtz Zentrum München, German Research Center for Environmental Health, Neuherberg, Germany ²⁵Institute of Molecular Animal Breeding and Biotechnology, Gene Center, Ludwig-Maximilians-University München, Munich, Germany ²⁶King's British Heart Foundation Centre, King's College London, London, UK ²⁷Department of Neurology, Medical University of Innsbruck, Innsbruck, Austria ²⁸Department of Public Health and Primary Care, University of Cambridge, Cambridge, UK ²⁹Department of Cardiovascular Physiology, Ruhr University Bochum, Bochum, Germany ³⁰Department of Biology, University of Padua, Padua, Italy ³¹Dulbecco-Telethon Institute, Venetian Institute of Molecular Medicine, Padua, Italy ³²Institute for Biology, Freie Universität Berlin, Berlin, Germany ³³NeuroCure, Charité, Berlin, Germany ³⁴Pôle de Biologie, Hôpital Européen Georges Pompidou, Paris, France ³⁵Karolinska Institute, Department of Women's and Children's Health, Karolinska University Hospital, Stockholm, Sweden ³⁶Department of Internal Medicine and Cardiology, German Heart Center Berlin, Berlin, Germany

Acknowledgements

We thank N. Mizushima (University of Tokyo, Tokyo, Japan) for providing *Atg5^{flox/flox}* mice and K. Chien (Harvard University, Cambridge, Massachusetts, USA) for providing *MLC2a-Cre* mice. We are grateful to R. Schreiber for assistance with high-resolution respirometry. FM is grateful to the Austrian Science Fund FWF (Austria) for grants P23490-B12, P24381, P 27893, I1000 and grant 'SFB Lipotox' and to BMWF and the Karl-Franzens University for grant 'Unkonventionelle Forschung'. S. Sedej is supported by the Austrian Science Fund FWF through grant P27637-B28 and by a grant from the Austrian Heart Foundation (Österreichischer Herzfonds). TE is recipient of an APART fellowship of the Austrian Academy of Sciences. MA received funding from the FWF (P27637-B28) and was trained within the frame of the PhD Program Molecular Medicine of the Medical University of Graz. SB is supported by the Austrian Science Fund FWF (grant P27183-B24) and Swedish Research Council (grant 2015-05468). JD is supported by the DFG via CRC1140 and by the Swiss National Science Foundation, grant 31003A-166482/1. PR is supported by the Austrian Science Fund (FWF) project J3742-B28 and NAWI Graz. WAL is supported by EU (FP7) program MEDIA and German Research Foundation, SFB1002, TPA8. GK is supported by the LeDucq Foundation, Cancéropôle Ile-de-France; Institut National du Cancer (INCa); the European Research Council (ERC); the LabEx Immuno-Oncology; and the Paris Alliance of Cancer Research Institutes (PACRI). The project was supported by grants from the Helmholtz Portfolio Theme 'Metabolic Dysfunction and Common Disease' (JB), the Helmholtz Alliance 'Imaging and Curing Environmental Metabolic Diseases (ICEMED)' (JB) and by the German Federal Ministry of Education and Research (Infrafrontier grant 01KX1012.) (MHA). SJS was supported by grants from the Bundesministerium für Bildung und Forschung (Smartage, 01GQ1420A), from the Forschungszentrum für neurodegenerative Erkrankungen and from the Deutsche Forschungsgemeinschaft (Exc 257). S.K., J.W., R.P., P.W. and M.M. are supported by an excellence initiative (Competence Centers for Excellent Technologies - COMET) of the Austrian Research Promotion Agency FFG: "Research Center of Excellence in Vascular Ageing – Tyrol, VASCage" (K-Project Nr. 843536) funded by the BMVIT, BMWF, the Wirtschaftsagentur Wien and the Standortagentur Tirol. This work was supported by the National Institute for Health Research (NIHR) Biomedical Research Centre based at Guy's and St Thomas' NHS Foundation Trust and King's College London in partnership with King's College Hospital. M.M. is a Senior Research fellow of the British Heart Foundation. The authors are grateful for the support by the animal facilities staff of the Institutes of Biomedical Research (IBF, Medical University of Graz) and Molecular Biosciences (IMB, University of Graz) and acknowledge the Center for Medical Research (ZMF) of the Medical University of Graz for technical assistance.

References

1. Zile MR, Brutsaert DL. New concepts in diastolic dysfunction and diastolic heart failure: Part I: diagnosis, prognosis, and measurements of diastolic function. *Circulation*. 2002; 105:1387–1393. [PubMed: 11901053]
2. Chiao YA, Rabinovitch PS. The Aging Heart. *Cold Spring Harb Perspect Med*. 2015; 5 a025148.
3. Redfield MM, et al. Burden of systolic and diastolic ventricular dysfunction in the community: appreciating the scope of the heart failure epidemic. *JAMA*. 2003; 289:194–202. [PubMed: 12517230]
4. Bui AL, Horwich TB, Fonarow GC. Epidemiology and risk profile of heart failure. *Nat Rev Cardiol*. 2011; 8:30–41. [PubMed: 21060326]
5. Nakai A, et al. The role of autophagy in cardiomyocytes in the basal state and in response to hemodynamic stress. *Nat Med*. 2007; 13:619–624. [PubMed: 17450150]
6. Taneike M, et al. Inhibition of autophagy in the heart induces age-related cardiomyopathy. *Autophagy*. 2010; 6:600–606. [PubMed: 20431347]
7. Madeo F, Zimmermann A, Maiuri MC, Kroemer G. Essential role for autophagy in life span extension. *J Clin Invest*. 2015; 125:85–93. [PubMed: 25654554]
8. Eisenberg T, et al. Induction of autophagy by spermidine promotes longevity. *Nat Cell Biol*. 2009; 11:1305–1314. [PubMed: 19801973]
9. Morselli E, et al. Spermidine and resveratrol induce autophagy by distinct pathways converging on the acetylproteome. *J Cell Biol*. 2011; 192:615–629. [PubMed: 21339330]
10. Gupta VK, et al. Restoring polyamines protects from age-induced memory impairment in an autophagy-dependent manner. *Nat Neurosci*. 2013; 16:1453–1460. [PubMed: 23995066]
11. Büttner S, et al. Spermidine protects against α -synuclein neurotoxicity. *Cell Cycle Georget Tex*. 2014; 13:3903–3908.

12. Wang I-F, et al. Autophagy activators rescue and alleviate pathogenesis of a mouse model with proteinopathies of the TAR DNA-binding protein 43. *Proc Natl Acad Sci U S A*. 2012; 109:15024–15029. [PubMed: 22932872]
13. Weindruch R, Walford RL, Fligiel S, Guthrie D. The retardation of aging in mice by dietary restriction: longevity, cancer, immunity and lifetime energy intake. *J Nutr*. 1986; 116:641–654. [PubMed: 3958810]
14. Dai D-F, et al. Overexpression of Catalase Targeted to Mitochondria Attenuates Murine Cardiac Aging. *Circulation*. 2009; 119:2789–2797. [PubMed: 19451351]
15. Blackwell BN, Bucci TJ, Hart RW, Turturro A. Longevity, body weight, and neoplasia in ad libitum-fed and diet-restricted C57BL6 mice fed NIH-31 open formula diet. *Toxicol Pathol*. 1995; 23:570–582. [PubMed: 8578100]
16. Treuting PM, et al. Reduction of age-associated pathology in old mice by overexpression of catalase in mitochondria. *J Gerontol A Biol Sci Med Sci*. 2008; 63:813–822. [PubMed: 18772469]
17. Soda K, Kano Y, Chiba F, Koizumi K, Miyaki Y. Increased polyamine intake inhibits age-associated alteration in global DNA methylation and 1,2-dimethylhydrazine-induced tumorigenesis. *PLoS One*. 2013; 8:e64357. [PubMed: 23696883]
18. Paulus WJ, et al. How to diagnose diastolic heart failure: a consensus statement on the diagnosis of heart failure with normal left ventricular ejection fraction by the Heart Failure and Echocardiography Associations of the European Society of Cardiology. *Eur Heart J*. 2007; 28:2539–2550. [PubMed: 17428822]
19. Ky B, et al. Ventricular-arterial coupling, remodeling, and prognosis in chronic heart failure. *J Am Coll Cardiol*. 2013; 62:1165–1172. [PubMed: 23770174]
20. Dai D-F, Rabinovitch PS. Cardiac aging in mice and humans: the role of mitochondrial oxidative stress. *Trends Cardiovasc Med*. 2009; 19:213–220. [PubMed: 20382344]
21. Heinzel FR, Hohendanner F, Jin G, Sedej S, Edelmann F. Myocardial Hypertrophy and Its Role in Heart Failure with Preserved Ejection Fraction. *J Appl Physiol Bethesda Md* 1985. 2015; jap. 00374.2015. doi: 10.1152/japphysiol.00374.2015
22. Linke WA, Hamdani N. Gigantic business: titin properties and function through thick and thin. *Circ Res*. 2014; 114:1052–1068. [PubMed: 24625729]
23. Borbély A, et al. Cardiomyocyte stiffness in diastolic heart failure. *Circulation*. 2005; 111:774–781. [PubMed: 15699264]
24. López-Otín C, Blasco MA, Partridge L, Serrano M, Kroemer G. The hallmarks of aging. *Cell*. 2013; 153:1194–1217. [PubMed: 23746838]
25. Salvioli S, et al. Inflamm-aging, cytokines and aging: state of the art, new hypotheses on the role of mitochondria and new perspectives from systems biology. *Curr Pharm Des*. 2006; 12:3161–3171. [PubMed: 16918441]
26. Duicu OM, et al. Ageing-induced decrease in cardiac mitochondrial function in healthy rats. *Can J Physiol Pharmacol*. 2013; 91:593–600. [PubMed: 23889593]
27. Liu Y, Samuel BS, Breen PC, Ruvkun G. Caenorhabditis elegans pathways that surveil and defend mitochondria. *Nature*. 2014; 508:406–410. [PubMed: 24695221]
28. Yeganeh B, et al. Targeting the mevalonate cascade as a new therapeutic approach in heart disease, cancer and pulmonary disease. *Pharmacol Ther*. 2014; 143:87–110. [PubMed: 24582968]
29. Paulus WJ, Tschöpe C. A novel paradigm for heart failure with preserved ejection fraction: comorbidities drive myocardial dysfunction and remodeling through coronary microvascular endothelial inflammation. *J Am Coll Cardiol*. 2013; 62:263–271. [PubMed: 23684677]
30. Haspel J, et al. Characterization of macroautophagic flux in vivo using a leupeptin-based assay. *Autophagy*. 2011; 7:629–642. [PubMed: 21460622]
31. Hariharan N, Zhai P, Sadoshima J. Oxidative stress stimulates autophagic flux during ischemia/reperfusion. *Antioxid Redox Signal*. 2011; 14:2179–2190. [PubMed: 20812860]
32. Shirakabe A, et al. Drp1-Dependent Mitochondrial Autophagy Plays a Protective Role Against Pressure Overload-Induced Mitochondrial Dysfunction and Heart Failure. *Circulation*. 2016; 133:1249–1263. [PubMed: 26915633]
33. Gottdiener JS, et al. Predictors of congestive heart failure in the elderly: the Cardiovascular Health Study. *J Am Coll Cardiol*. 2000; 35:1628–1637. [PubMed: 10807470]

34. Doi R, et al. Development of different phenotypes of hypertensive heart failure: systolic versus diastolic failure in Dahl salt-sensitive rats. *J Hypertens*. 2000; 18:111–120. [PubMed: 10678551]
35. Qu P, et al. Time-course changes in left ventricular geometry and function during the development of hypertension in Dahl salt-sensitive rats. *Hypertens Res Off J Jpn Soc Hypertens*. 2000; 23:613–623.
36. Palmer RM, Ashton DS, Moncada S. Vascular endothelial cells synthesize nitric oxide from L-arginine. *Nature*. 1988; 333:664–666. [PubMed: 3131684]
37. Chen PY, Sanders PW. L-arginine abrogates salt-sensitive hypertension in Dahl/Rapp rats. *J Clin Invest*. 1991; 88:1559–1567. [PubMed: 1658045]
38. Tang WHW, Wang Z, Cho L, Brennan DM, Hazen SL. Diminished global arginine bioavailability and increased arginine catabolism as metabolic profile of increased cardiovascular risk. *J Am Coll Cardiol*. 2009; 53:2061–2067. [PubMed: 19477356]
39. Sourij H, et al. Arginine bioavailability ratios are associated with cardiovascular mortality in patients referred to coronary angiography. *Atherosclerosis*. 2011; 218:220–225. [PubMed: 21632053]
40. Ommen SR, et al. Clinical utility of Doppler echocardiography and tissue Doppler imaging in the estimation of left ventricular filling pressures: A comparative simultaneous Doppler-catheterization study. *Circulation*. 2000; 102:1788–1794. [PubMed: 11023933]
41. Torre-Amione G. Immune activation in chronic heart failure. *Am J Cardiol*. 2005; 95:3C–8C. discussion 38C–40C.
42. Kelly RP, et al. Effective arterial elastance as index of arterial vascular load in humans. *Circulation*. 1992; 86:513–521. [PubMed: 1638719]
43. Leoncini G, et al. Renal and cardiac abnormalities in primary hypertension. *J Hypertens*. 2009; 27:1064–1073. [PubMed: 19357534]
44. Gori M, et al. Association between renal function and cardiovascular structure and function in heart failure with preserved ejection fraction. *Eur Heart J*. 2014; 35:3442–3451. [PubMed: 24980489]
45. Klotz S, et al. Development of heart failure in chronic hypertensive Dahl rats: focus on heart failure with preserved ejection fraction. *Hypertension*. 2006; 47:901–911. [PubMed: 16585423]
46. Mori K, Nakao K. Neutrophil gelatinase-associated lipocalin as the real-time indicator of active kidney damage. *Kidney Int*. 2007; 71:967–970. [PubMed: 17342180]
47. Stegemann C, et al. Lipidomics profiling and risk of cardiovascular disease in the prospective population-based Bruneck study. *Circulation*. 2014; 129:1821–1831. [PubMed: 24622385]
48. Schindler CE, Partap U, Patchen BK, Swoap SJ. Chronic rapamycin treatment causes diabetes in male mice. *Am J Physiol Regul Integr Comp Physiol*. 2014; 307:R434–443. [PubMed: 24965794]
49. Miller RA, et al. Rapamycin-mediated lifespan increase in mice is dose and sex dependent and metabolically distinct from dietary restriction. *Aging Cell*. 2014; 13:468–477. [PubMed: 24341993]
50. LaRocca TJ, Gioscia-Ryan RA, Hearon CM Jr, Seals DR. The autophagy enhancer spermidine reverses arterial aging. *Mech Ageing Dev*.
51. García-Prat L, et al. Autophagy maintains stemness by preventing senescence. *Nature*. 2016; 529:37–42. [PubMed: 26738589]
52. Hara T, et al. Suppression of basal autophagy in neural cells causes neurodegenerative disease in mice. *Nature*. 2006; 441:885–889. [PubMed: 16625204]
53. Wettschureck N, et al. Absence of pressure overload induced myocardial hypertrophy after conditional inactivation of Galphaq/Galpa11 in cardiomyocytes. *Nat Med*. 2001; 7:1236–1240. [PubMed: 11689889]
54. Sedej S, et al. Na⁺-dependent SR Ca²⁺ overload induces arrhythmogenic events in mouse cardiomyocytes with a human CPVT mutation. *Cardiovasc Res*. 2010; 87:50–59. [PubMed: 20080988]
55. Miller RA, et al. An aging Interventions Testing Program: study design and interim report. *Aging Cell*. 2007; 6:565–575. [PubMed: 17578509]

56. Yuan R, et al. Aging in inbred strains of mice: study design and interim report on median lifespans and circulating IGF1 levels. *Aging Cell*. 2009; 8:277–287. [PubMed: 19627267]
57. Kastenmayer RJ, Fain MA, Perdue KA. A retrospective study of idiopathic ulcerative dermatitis in mice with a C57BL/6 background. *J Am Assoc Lab Anim Sci JAALAS*. 2006; 45:8–12.
58. Rozman J, et al. Glucose tolerance tests for systematic screening of glucose homeostasis in mice. *Curr Protoc Mouse Biol*. 2015; 5:65–84. [PubMed: 25727201]
59. Sedej S, et al. Subclinical abnormalities in sarcoplasmic reticulum Ca(2+) release promote eccentric myocardial remodeling and pump failure death in response to pressure overload. *J Am Coll Cardiol*. 2014; 63:1569–1579. [PubMed: 24315909]
60. Troy BL, Pombo J, Rackley CE. Measurement of left ventricular wall thickness and mass by echocardiography. *Circulation*. 1972; 45:602–611. [PubMed: 4258936]
61. Pacher P, Nagayama T, Mukhopadhyay P, Bátkai S, Kass DA. Measurement of cardiac function using pressure-volume conductance catheter technique in mice and rats. *Nat Protoc*. 2008; 3:1422–1434. [PubMed: 18772869]
62. Tournoux F, et al. Validation of noninvasive measurements of cardiac output in mice using echocardiography. *J Am Soc Echocardiogr Off Publ Am Soc Echocardiogr*. 2011; 24:465–470.
63. Abdellatif M, et al. Spectral transfer function analysis of respiratory hemodynamic fluctuations predicts end-diastolic stiffness in preserved ejection fraction heart failure. *Am J Physiol Heart Circ Physiol*. 2016; 310:H4–13. [PubMed: 26475584]
64. Wolf D, et al. CD4+CD25+ regulatory T cells inhibit experimental anti-glomerular basement membrane glomerulonephritis in mice. *J Am Soc Nephrol JASN*. 2005; 16:1360–1370. [PubMed: 15788479]
65. Saeed AI, et al. TM4: a free, open-source system for microarray data management and analysis. *BioTechniques*. 2003; 34:374–378. [PubMed: 12613259]
66. Sturn A, Quackenbush J, Trajanoski Z. Genesis: cluster analysis of microarray data. *Bioinforma Oxf Engl*. 2002; 18:207–208.
67. Shevchenko A, Tomas H, Havlis J, Olsen JV, Mann M. In-gel digestion for mass spectrometric characterization of proteins and proteomes. *Nat Protoc*. 2006; 1:2856–2860. [PubMed: 17406544]
68. Rappsilber J, Mann M, Ishihama Y. Protocol for micro-purification, enrichment, pre-fractionation and storage of peptides for proteomics using StageTips. *Nat Protoc*. 2007; 2:1896–1906. [PubMed: 17703201]
69. Sprenger A, Küttner V, Bruckner-Tuderman L, Dengjel J. Global proteome analyses of SILAC-labeled skin cells. *Methods Mol Biol Clifton NJ*. 2013; 961:179–191.
70. Cox J, Mann M. MaxQuant enables high peptide identification rates, individualized p.p.b.-range mass accuracies and proteome-wide protein quantification. *Nat Biotechnol*. 2008; 26:1367–1372. [PubMed: 19029910]
71. Magnes C, et al. Polyamines in biological samples: rapid and robust quantification by solid-phase extraction online-coupled to liquid chromatography-tandem mass spectrometry. *J Chromatogr A*. 2014; 1331:44–51. [PubMed: 24485539]
72. Yuan M, Breitkopf SB, Yang X, Asara JM. A positive/negative ion-switching, targeted mass spectrometry-based metabolomics platform for bodily fluids, cells, and fresh and fixed tissue. *Nat Protoc*. 2012; 7:872–881. [PubMed: 22498707]
73. Braun RJ, et al. Accumulation of Basic Amino Acids at Mitochondria Dictates the Cytotoxicity of Aberrant Ubiquitin. *Cell Rep*. 2015; doi: 10.1016/j.celrep.2015.02.009
74. Buescher JM, Moco S, Sauer U, Zamboni N. Ultrahigh performance liquid chromatography-tandem mass spectrometry method for fast and robust quantification of anionic and aromatic metabolites. *Anal Chem*. 2010; 82:4403–4412. [PubMed: 20433152]
75. Roth M. Fluorescence reaction for amino acids. *Anal Chem*. 1971; 43:880–882. [PubMed: 5576608]
76. Schwarz EL, Roberts WL, Pasquali M. Analysis of plasma amino acids by HPLC with photodiode array and fluorescence detection. *Clin Chim Acta Int J Clin Chem*. 2005; 354:83–90.
77. Shirakabe A, et al. Evaluating mitochondrial autophagy in the mouse heart. *J Mol Cell Cardiol*. 2016; 92:134–139. [PubMed: 26868976]

78. Neagoe C. Titin Isoform Switch in Ischemic Human Heart Disease. *Circulation*. 2002; 106:1333–1341. [PubMed: 12221049]
79. Hamdani N, et al. Crucial role for Ca²⁺/calmodulin-dependent protein kinase-II in regulating diastolic stress of normal and failing hearts via titin phosphorylation. *Circ Res*. 2013; 112:664–674. [PubMed: 23283722]
80. Mayhew TM. Taking tissue samples from the placenta: an illustration of principles and strategies. *Placenta*. 2008; 29:1–14. [PubMed: 17658596]
81. Mühlfeld C, Nyengaard JR, Mayhew TM. A review of state-of-the-art stereology for better quantitative 3D morphology in cardiac research. *Cardiovasc Pathol Off J Soc Cardiovasc Pathol*. 2010; 19:65–82.
82. Méndez J, Keys A. Density and composition of mammalian muscle. *Metabolism*. 1960; 9:184–188.
83. Willett WC, et al. Reproducibility and validity of a semiquantitative food frequency questionnaire. *Am J Epidemiol*. 1985; 122:51–65. [PubMed: 4014201]
84. McKee PA, Castelli WP, McNamara PM, Kannel WB. The natural history of congestive heart failure: the Framingham study. *N Engl J Med*. 1971; 285:1441–1446. [PubMed: 5122894]
85. Willeit P, et al. Discrimination and net reclassification of cardiovascular risk with lipoprotein(a): prospective 15-year outcomes in the Bruneck Study. *J Am Coll Cardiol*. 2014; 64:851–860. [PubMed: 25169167]
86. Willett W, Stampfer MJ. Total energy intake: implications for epidemiologic analyses. *Am J Epidemiol*. 1986; 124:17–27. [PubMed: 3521261]
87. Assarsson E, et al. Homogenous 96-plex PEA immunoassay exhibiting high sensitivity, specificity, and excellent scalability. *PloS One*. 2014; 9:e95192. [PubMed: 24755770]
88. Wei J, Carroll RJ, Harden KK, Wu G. Comparisons of treatment means when factors do not interact in two-factorial studies. *Amino Acids*. 2012; 42:2031–2035. [PubMed: 21547361]
89. Burkhoff D, Mirsky I, Suga H. Assessment of systolic and diastolic ventricular properties via pressure-volume analysis: a guide for clinical, translational, and basic researchers. *Am J Physiol Heart Circ Physiol*. 2005; 289:H501–512. [PubMed: 16014610]

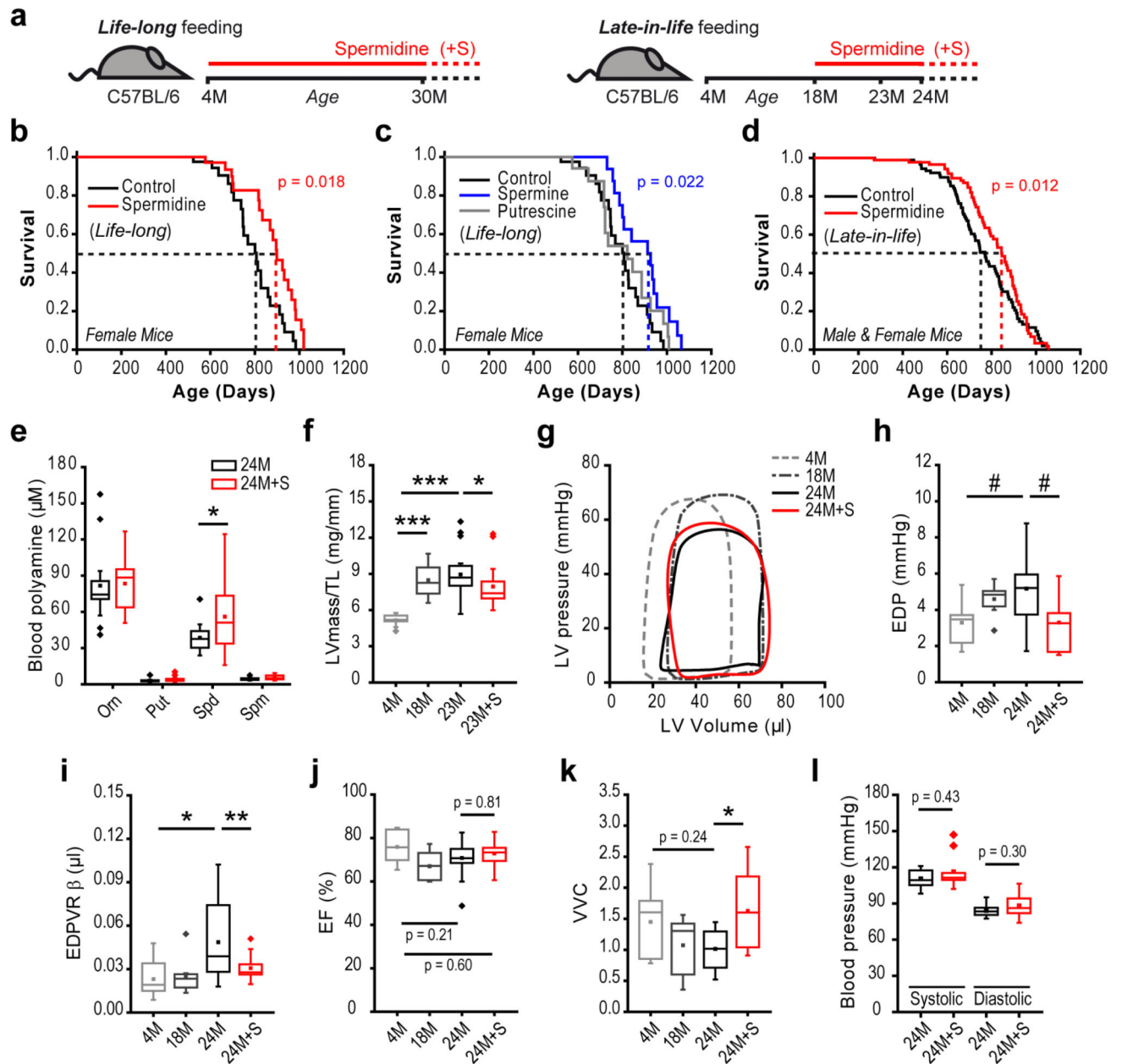


Figure 1. Spermidine extends lifespan and improves cardiac diastolic function in mice.

(a) Schematic overview of spermidine administration to aging wild-type C57BL/6J mice.

Spermidine was supplemented to drinking water starting from the age of 4 months (*life-long*) or 18 months (*late-in-life*) and cardiovascular parameters (Fig. 1f-l) or molecular phenotypes (Figs. 2 and 3) were analyzed at the indicated time points (M, months).

(b-d) Kaplan-Meier survival analyses. In the *life-long* supplementation experiment using C57BL/6J female mice **(b, c)**, the same control group was used. The *late-in-life* supplementation experiment **(d)** used C57BL/6J male and female mice. Dashed lines depict median lifespans. $N=40/41$ **(b, control/spermidine)**, $N=40/20/17$ **(c, control/putrescine/**

spermine), N=91/86 (**d**, control/spermidine) mice (see Supplementary Tables 1 and 2 for more details). P-values, calculated using Breslow test, represent pairwise comparisons of survival curves between the groups *Spermidine* vs. *Control* (**b**), *Spermine* vs. *Control* (**c**), and *Spermidine* vs. *Control* (**d**).

(**e-k**) Effects of *late-in-life* supplementation of spermidine in C57BL6/J male mice, analyzed at the indicated ages (M, months). Shown are whole blood polyamine levels (**e**), left ventricular mass-to-tibia length ratio (LVmass/TL), indicative of cardiac hypertrophy (**f**), representative hemodynamic pressure-volume loops (**g**), left ventricular end-diastolic pressure (EDP) (**h**), myocardial stiffness constant (end-diastolic pressure-volume relationship [EDPVR] β obtained from exponential fits presented in Supplementary Fig. 4a) (**i**), ejection fraction, as determined by echocardiography (**j**) and ventricular-vascular coupling (VVC) (**k**). N=15/18 (**e**, 24M/24M+S), N=10/14/20/20 (**f, j**, 4M/18M/23M/23M+S), N=10/8/10/10 (**h, i, k**, 4M/18M/24M/24M+S) mice.

(**l**) Systolic and diastolic arterial blood pressures in mice analyzed in (**e**). N=8/11 (**l**, 24M/24M+S) mice.

*** $p < 0.001$, ** $p < 0.01$, * $p < 0.05$ and # $p < 0.06$ (ANOVA with post-hoc Tukey, ANCOVA (panel i) or Welch's *t*-test (panel e), see Methods). For box-and-whisker plots, whiskers show minima and maxima within 1.5 interquartile range.

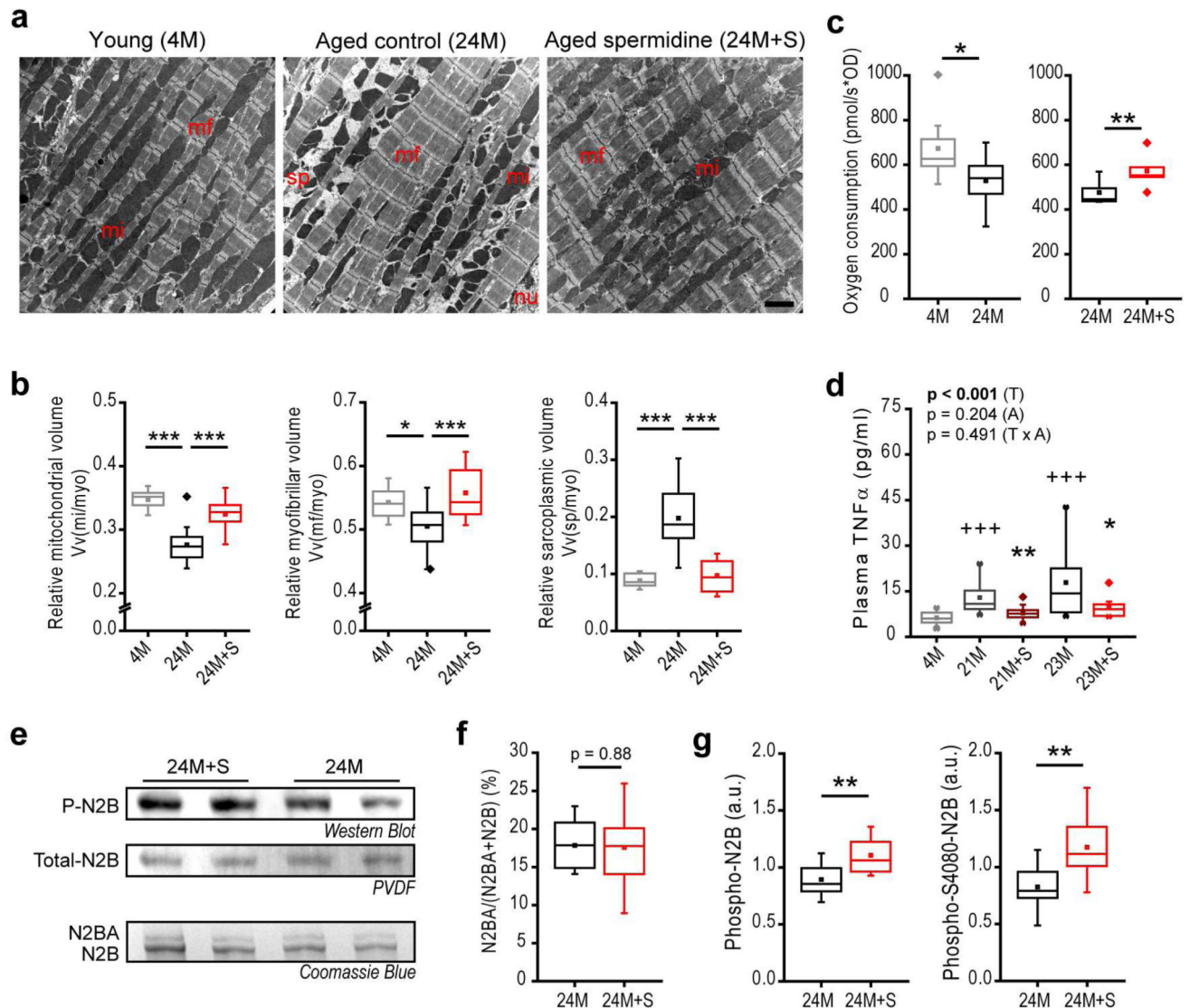


Figure 2. Spermidine improves cardiomyocyte composition and mitochondrial function in mice. C57BL/6J male mice were supplemented with spermidine (+S) *late-in-life* (see Fig. 1a for the feeding scheme) and hearts were subjected to molecular and biochemical analyses at the indicated ages (M, months).

(a, b) Representative transmission electron micrographs (a) and quantification of left ventricular cardiomyocyte composition using design-based stereology (b). Relative volumes of mitochondria $Vv(mi/myo)$, myofibrils $Vv(mf/myo)$ and mitochondria- and myofibril-free sarcoplasm $Vv(sp/myo)$ per cardiomyocyte are shown. *mi*, mitochondria; *mf*, myofibrils; *myo*, cardiomyocyte; *nu*, nucleus; *sp*, sarcoplasm. Scale bar represents 2 μ m. N=10/15/14 (4M/24M/24M+S) mice.

(c) Oxygen consumption (complex I-mediated respiration) of isolated cardiac mitochondria using high-resolution respirometry. N=8 (left), N=5 (right) mice/group.

(d) Plasma TNF α levels after *late-in-life* spermidine supplementation of C57BL6/J male mice. Mice that had a possibly acute inflammatory condition were excluded (see Supplementary Fig. 8 and Methods). N=12/12/13/9/10 (5M/21M/21M+S/23M/23M+S) mice.

(e) Titin isoform composition and phosphorylation. Representative *Western Blots* probed with a pan-phospho-serine/threonine-antibody for detection of total N2B phosphorylation (P-N2B, quantified in g), Coomassie-stained *PVDF* membrane for detection of total N2B (*Total-N2B*), and a *Coomassie Blue*-stained gel for detection of N2BA and N2B isoforms quantified in f (see Methods for details on isoform identification).

(f) The N2BA/(N2BA+N2B) ratio was quantified by densitometry using normalization standards for inter-gel comparisons (see Methods). (N=12 mice/group).

(g) Quantification of total N2B phosphorylation (left) and serine 4080 (S4080)-specific N2B phosphorylation (right, from densitometry of western blots representatively shown in Supplementary Fig. 5c). (N=12 mice/group).

Panels b,c, f,g: ***p<0.001, **p<0.01 and *p<0.05 (ANOVA with post-hoc Tukey, Welch's test with post-hoc Games-Howell or *t*-test (paired in panel c) as appropriate, see Methods).

Panel d: P-value represent factor (T, treatment; A, age) comparisons by two-way ANOVA including 21M and 23M groups followed by simple main effects (**p<0.01, *p<0.05 vs. age-matched control); +++p<0.001 (ANOVA post-hoc Tukey comparing controls). For box-and-whisker plots, whiskers show minima and maxima within 1.5 interquartile range.

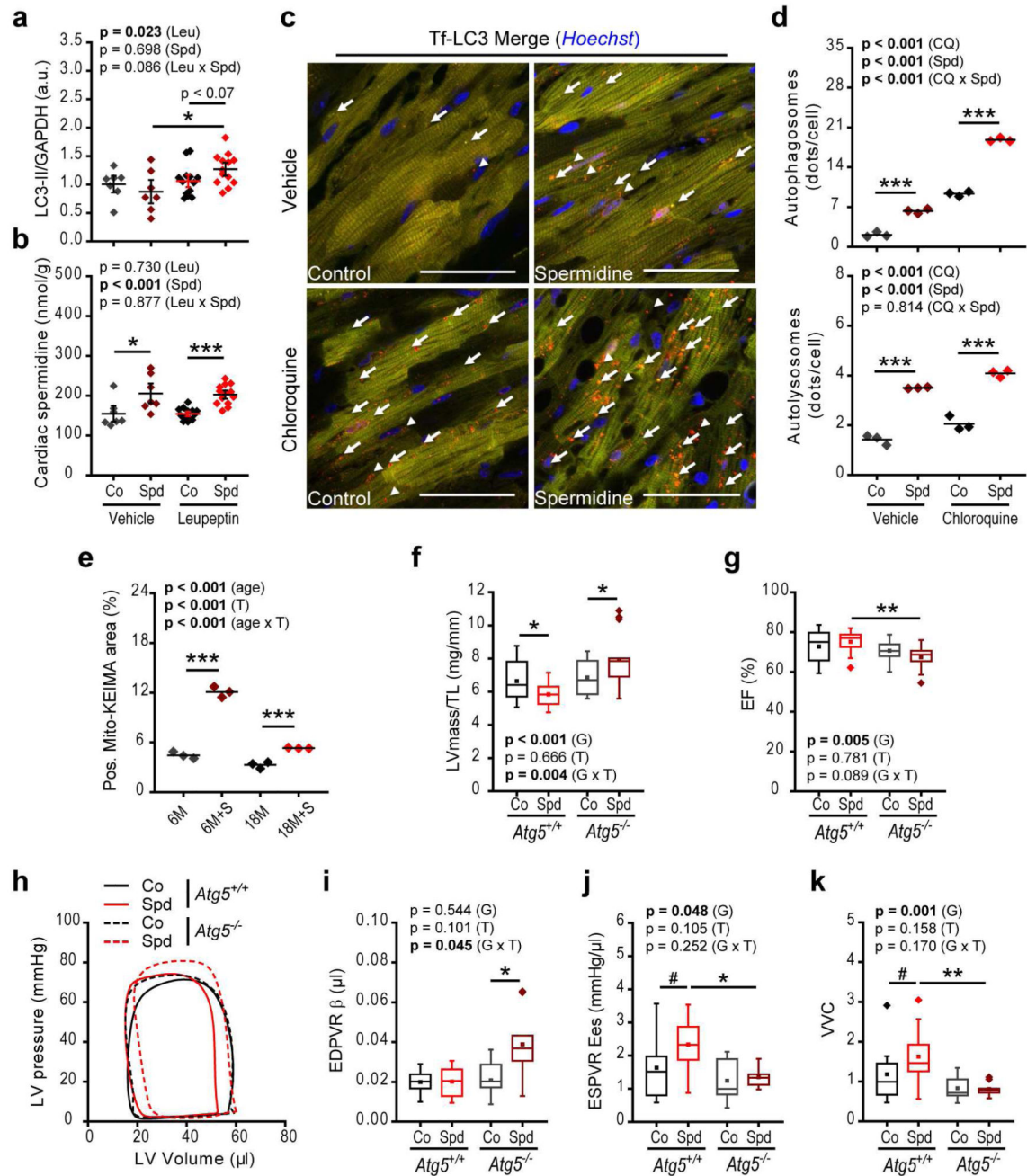


Figure 3. Spermidine ameliorates cardiac function through induction of autophagy.

(a, b) Cardiac autophagic flux assessed by the LC3-II/GAPDH ratio, determined using western blot analysis (Supplementary Fig. 9e) (a) and cardiac tissue levels of spermidine (b) 50 min after intraperitoneal injection of leupeptin or vehicle in 13-month-old C57BL/6J male mice with or without 4 weeks of spermidine supplementation to the drinking water. N=7/13 (Vehicle/Leu) mice/group. Co, Control; Spd, Spermidine; Leu, Leupeptin. (c, d) Young (3-month-old) transgenic mice harboring cardiac-specific expressed tandem-fluorescence mRFP-GFP-LC3 (tf-LC3) were subjected to spermidine treatment for 2 weeks

and hearts were analyzed by confocal microscopy 4 hours after intraperitoneal injection of chloroquine (CQ) or vehicle to assess autophagic flux. Representative RFP/GFP/*Hoechst* overlays (**c**) and quantification of autophagosomes (orange puncta in **c**, **arrows**) and autolysosomes (red puncta in **c**, **arrowheads**) (**d**) are shown. Scale bars represent 50 μm . N=3 mice/group.

(e) Mitophagy was assessed in young (6-month-old) or aged (18-month-old) C57BL/6J wild-type mice treated with or without 2 weeks of spermidine supplementation and injected with AAV9-Mito-Keima. The positive ratiometric area (see Supplementary Fig. 9b-d) of Mito-Keima fluorescence (561 nm/457 nm excitation), indicative of mitophagy, was quantified. N=3 mice/group.

(f-k) Cardiomyocyte-specific *Atg5*-deficient mice (*Atg5*^{-/-}) were analyzed at 16 weeks of age and compared to age-matched *Atg5*^{+/+} littermates, with or without 12 weeks of spermidine supplementation (see Supplementary Fig. 10). Shown are tibia length-normalized left ventricular mass (LVmass/TL) (**f**), ejection fraction (EF) (**g**), representative pressure-volume loops (**h**), myocardial stiffness constant (end-diastolic pressure-volume relationships [EDPVR] β obtained from exponential fits, Supplementary Fig. 10d) (**i**), end-systolic elastance (Ees, slope of the end-systolic pressure-volume relationship, Supplementary Fig. 10e) (**j**) and ventricular-vascular coupling (VVC) (**k**). N=16/15 and N=12/14 (**f**, **g**, Co/Spd) mice, *Atg5*^{+/+} and *Atg5*^{-/-}, respectively. N=10/10 and N=9/11 (**i-k**, Co/Spd) mice, *Atg5*^{+/+} and *Atg5*^{-/-}, respectively.

P-values represent factor (T, treatment; G, genotype) comparisons by two-way ANOVA (ANCOVA in panel i) followed by simple main effects (**p<0.001, *p<0.01, #p<0.05 and #p<0.06). Dot-plots show means \pm s.e.m. For box-and-whisker plots, whiskers show minima and maxima within 1.5 interquartile range.

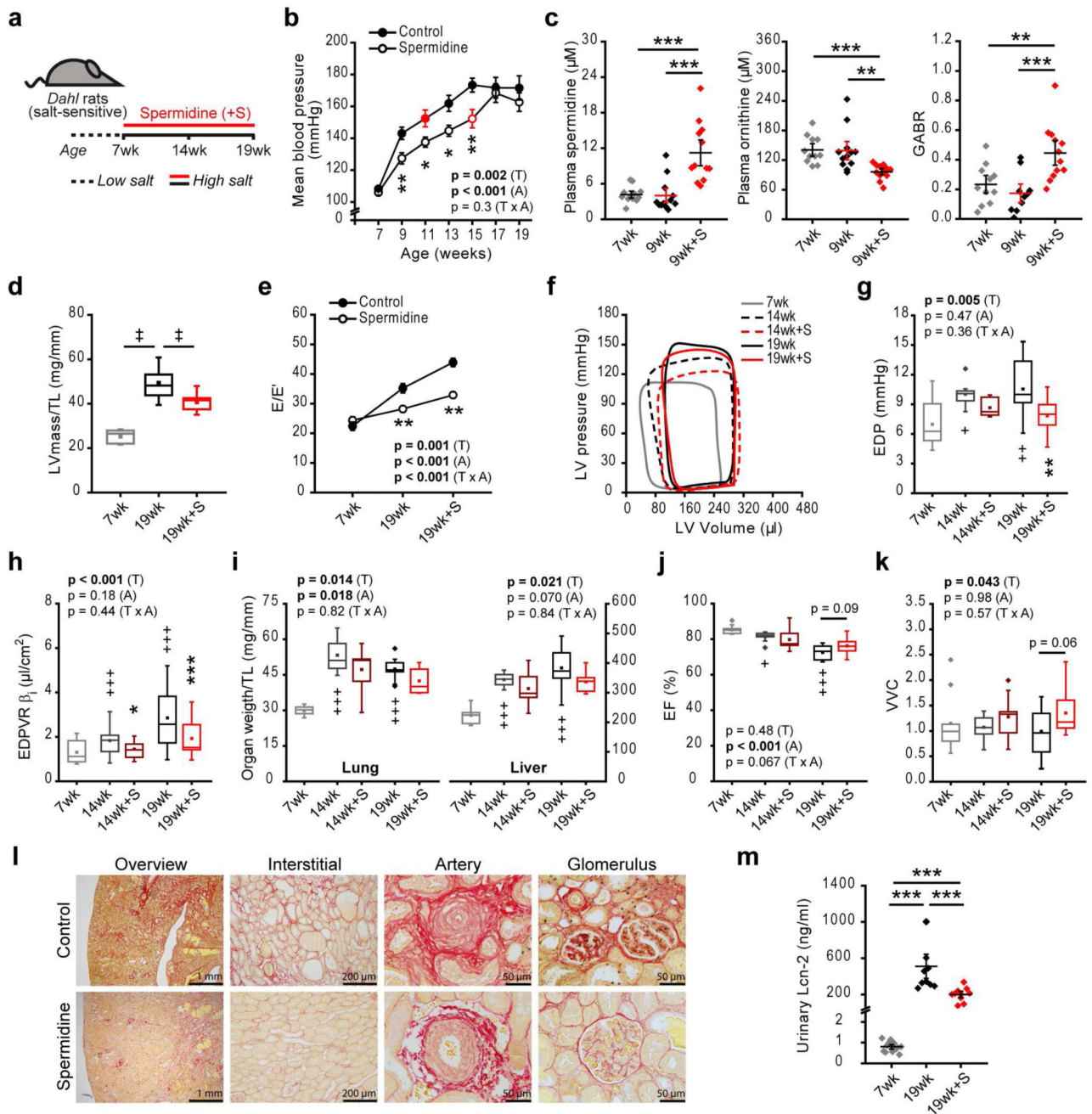


Figure 4. Spermidine ameliorates salt-induced hypertension and heart failure in *Dahl* salt-sensitive rats.

(a) Schematic overview of spermidine administration (starting from the age of 7 weeks) to *Dahl* salt-sensitive rats fed a high-salt diet (8% NaCl) *ad libitum*. Cardiovascular parameters

(b-k) and renal tissue characteristics (l, m) were recorded at the indicated ages. (b) Mean arterial blood pressure (MBP) by the non-invasive tail-cuff method. (N=10 rats/group). Red symbols denote the first time point at which there is a non-significant difference in MBP compared to the peak MBP of the group.

(c) Plasma spermidine and ornithine content and global arginine bioavailability ratio (GABR). N=12/12/12, 11/12/12, 11/12/10 (7wk/9wk/9wk+S) rats, left, center and right sub-panels, respectively.

(d, e) Echocardiographic assessment of tibia length-normalized LV mass (LVmass/TL) **(d)** and the ratio of peak early Doppler transmitral flow velocity (E) to the corresponding myocardial tissue Doppler velocity (E') **(e)**. N=10 rats/group.

(f-k) Representative pressure-volume loops **(f)**, LV end-diastolic pressure (EDP) **(g)**, myocardial stiffness constant for indexed volumes (end-diastolic pressure-volume relationship [EDPVR] β_i) **(h)**, tibia length (TL)-normalized lung and liver weights **(i)**, ejection fraction (EF) **(j)**, and ventricular-vascular coupling (VVC) **(k)**. N=10/9/9/10/10 (7wk/14wk/14wk+S/19wk/19wk+S) rats.

(l) Representative micrographs of 9 rats/group analyzed for renal fibrosis in 19-week-old rats, as assessed by picrosirius red collagen staining.

(m) Urinary lipocalin-2 (Lcn-2) levels. N=12/10/10 (7wk/19wk/19wk+S) rats.

*** $p < 0.001$, ** $p < 0.01$ and * $p < 0.05$ (ANOVA with post-hoc Tukey in panel c, m, Kruskal-Wallis with corrected multiple-comparisons in panel d). Panels b, e, g-k: p-values represent factor (T, treatment; A, age) comparisons by two-way ANOVA (mixed-design in b and e) including 14wk and 19wk groups followed by simple main effects (*** $p < 0.001$, ** $p < 0.01$, * $p < 0.05$ vs. age-matched control); +++ $p < 0.001$, ++ $p < 0.01$, + $p < 0.05$ (ANOVA with post-hoc Tukey comparing controls). Dot- and line-plots show means \pm s.e.m. For box-and-whisker plots, whiskers show minima and maxima within 1.5 interquartile range.

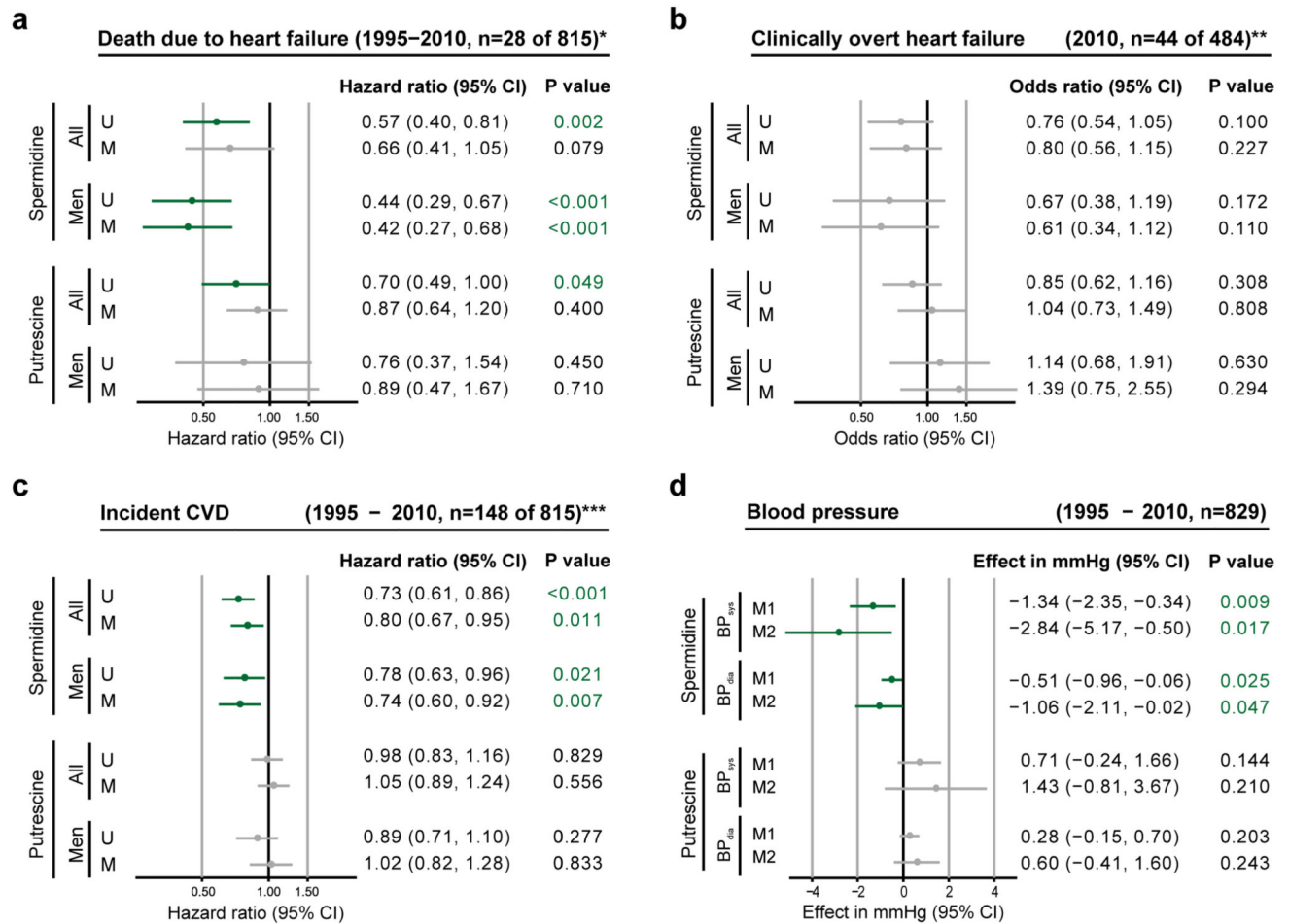


Figure 5. Dietary spermidine intake inversely correlates with human cardiovascular disease. (a-c) Associations of polyamine intake (spermidine or putrescine) in human subjects with death due to heart failure (a), clinically overt heart failure (b) and incident cardiovascular disease (CVD, a composite of acute coronary artery disease, stroke and death to due vascular disease) (c). Hazard ratios (a and c, time-to-event analysis) and odds ratios (b, cross-sectional analysis) are indicated for one standard deviation higher intake of the given polyamine. Models were unadjusted (U) or had multivariable adjustment (M) for age, sex, total caloric intake, current smoking, diabetes, alcohol consumption, and diastolic blood pressure. *Death due to heart failure was defined according to the International Statistical Classification of Diseases and Related Health Problems, 10th revision (ICD-10) codes I50.x, I13.0, I13.2, I11.00, I11.01, or I97.1, and the results represent sub-distribution hazard ratios based on the Fine and Gray model and account for the competing risk of death due to causes unrelated to heart failure. **Diagnosis of clinically overt heart failure (ascertained in 2010) relied on gold standard Framingham criteria. ***See methods for incident CVD criteria. (d) Association of polyamine (spermidine or putrescine) intake with systolic (BP_{sys}) and diastolic (BP_{dia}) blood pressures repeatedly assessed in 829 participants of the Bruneck Study (1995-2010). The effects shown represent the average difference in blood pressure (mmHg) associated with one standard deviation higher intake of the given polyamine (M1)

or between the first and third tertile groups (M2) under adjustment for age, sex, and total caloric intake.

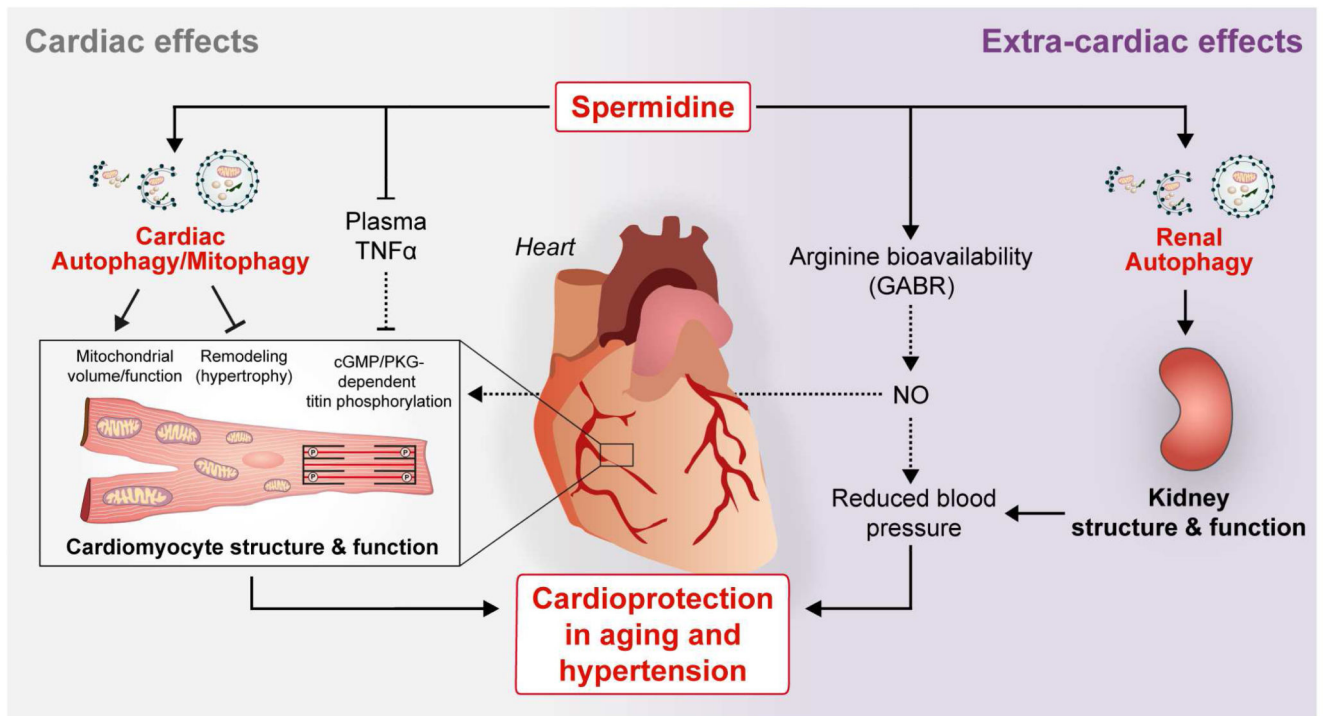


Figure 6. Mechanistic model of spermidine-mediated cardioprotection in aging and hypertensive heart failure.

Oral (dietary) supplementation of spermidine improves cardiac function by (i) promoting protective autophagy and mitophagy in cardiomyocytes; (ii) reducing subclinical, chronic inflammation (circulating TNF α levels) that impinges on cardiomyocyte function; (iii) improving systemic arginine bioavailability that may favor the production of the vasodilator nitric oxide (NO), and thus decrease systemic blood pressure; and (iv) inhibiting kidney damage through induction of autophagy. Improved renal function by spermidine treatment may additionally contribute to reduced arterial blood pressure and cardioprotection in the setting of salt-induced hypertension. In conjunction with spermidine's anti-inflammatory action, its autophagy-dependent effects on cardiomyocytes lead to enhanced mitochondrial volume and function, increased titin phosphorylation and reduced hypertrophy, which in turn result in improved mechano-elastic properties of cardiomyocytes.